NASA Technical Paper 3624

June 1996

The X-31A Quasi-Tailless Flight Test Results

John T. Bosworth and
P. C. Stoliker

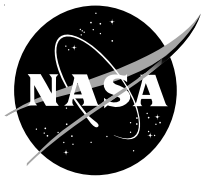

NASA Technical Paper 3624

1996

The X-31A Quasi-Tailless Flight Test Results

John T. Bosworth and P. C. Stoliker
Dryden Flight Research Center
Edwards, California

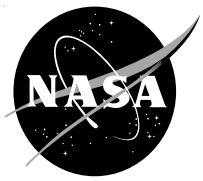

National Aeronautics and Space Administration

Office of Management

Scientific and Technical Information Program

A quasi-tailless flight investigation was launched using the X-31A enhanced fighter maneuverability airplane. In-flight simulations were used to assess the effect of partial to total vertical tail removal. The rudder control surface was used to cancel the stabilizing effects of the vertical tail, and yaw thrust vector commands were used to restabilize and control the airplane. The quasi-tailless mode was flown supersonically with gentle maneuvering and subsonically in precision approaches and ground attack profiles. Pilot ratings and a full set of flight test measurements were recorded. This report describes the results obtained and emphasizes the lessons learned from the X-31A flight test experiment. Sensor-related issues and their importance to a quasi-tailless simulation and to ultimately controlling a directionally unstable vehicle are assessed. The X-31A quasi-tailless flight test experiment showed that tailless and reduced tail fighter aircraft are definitely feasible. When the capability is designed into the airplane from the beginning, the benefits have the potential to outweigh the added complexity required.

ABSTRACT

A quasi-tailless flight investigation was launched using the X-31A enhanced fighter maneuverability airplane. In-flight simulations were used to assess the effect of partial to total vertical tail removal. The rudder control surface was used to cancel the stabilizing effects of the vertical tail, and yaw thrust vector commands were used to restabilize and control the airplane. The quasi-tailless mode was flown supersonically with gentle maneuvering and subsonically in precision approaches and ground attack profiles. Pilot ratings and a full set of flight test measurements were recorded. This report describes the results obtained and emphasizes the lessons learned from the X-31A flight test experiment. Sensor-related issues and their importance to a quasi-tailless simulation and to ultimately controlling a directionally unstable vehicle are assessed. The X-31A quasi-tailless flight test experiment showed that tailless and reduced tail fighter aircraft are definitely feasible. When the capability is designed into the airplane from the beginning, the benefits have the potential to outweigh the added complexity required.

INTRODUCTION

Early aircraft designers realized the necessity of using a vertical tail to provide directionally stable airplane designs. This practice has carried through to modern commercial and military aircraft designs, the majority of which include vertical tails and rudder control surfaces. For transport aircraft, the need to control the large yawing moments created in an engine failure condition dictates tail size. With the advent of thrust vectoring and full-authority flight control systems, significantly reducing or eliminating the vertical tail became a viable design option.

Potential advantages of a reduced tail size include decreased drag, reduced weight, and reduced structural complexity. For military applications, reduced radar cross-section is an additional advantage. These advantages must be balanced against the disadvantages of the added weight, complexity, and reliability requirements of a thrust vector system. If sufficient thrust vectoring system reliability cannot be achieved, emergency systems may also be required. In addition, because the thrust vector control power is proportional to the engine power setting, some flight conditions that normally require low-power settings, such as landing, may require larger drag devices, such as speed brakes, to maintain necessary higher power settings.

The X-31A enhanced fighter maneuverability airplane provided a unique opportunity to demonstrate the ability of a thrust vector system to provide the stabilizing and maneuvering moments equal to that of a vertical tail and rudder (refs. 1-5). A quasi-tailless investigation was launched which used destabilizing feedbacks to the rudder for in-flight simulation of partial to total vertical tail removal. The rudder control surface was used to cancel the stabilizing effects of the vertical tail, and yaw thrust vector deflections were used to restabilize and directionally control the aircraft.

This report summarizes the observations and lessons learned from the X-31A quasi-tailless flight experiment. The quasi-tailless mode was flown at one supersonic flight condition with high power settings and in a large subsonic flight envelope with reduced power settings. Handling qualities assessments were made using a precision approach and landing task and a simulated ground attack task. Pilot ratings and a full set of flight test measurements were recorded during the experiment. These measurements included pilot inputs, aircraft response, and control surface activity. Comparisons between the simulation-predicted results and flight test results are presented. Emphasis is placed on areas where differences were observed.

NOMENCLATURE

Acronyms

AGL	above ground level
AOA	angle of attack
ARPA	Advanced Research Projects Agency
ATLAS	Adaptable Target Lighting Array System
CHR	Cooper–Harper rating
CIC	close in combat
DASA	Daimler-Benz Aerospace, Germany
EFM	enhanced fighter maneuverability
FMOD	Federal Ministry of Defense, Germany
FORTRAN	Formula translation
FQ	flying qualities
HARV	High Angle of Attack Research Vehicle
JAST	Joint Advanced Strike Technology
KIAS	knots indicated airspeed
NASA	National Aeronautics and Space Administration
PLA	power lever angle
QT	quasi-tailless
RI	Rockwell International, Downey, California
TC	test conductor
USAF	United States Air Force
USN	United States Navy

Symbols

A	state derivative matrix
B	control derivative matrix
$c_{n_{\delta R}}$	rudder surface yaw control effectiveness derivative
$c_{n_{TVV}}$	thrust vector system yaw control effectiveness derivative
destab	destabilization
g	unit of acceleration, 32.174 ft/sec^2
K	destabilization feedback gain matrix
p	roll rate, deg/sec
r	yaw rate, deg/sec
u	control input vector
x	state vector
β	angle of sideslip, deg
δ_{df}	differential flap position, deg

δ_R	rudder position, deg
δ_{TVV}	thrust vector deflection, deg
ϕ	angle of bank, deg

Subscripts and Superscripts

$\dot{\ }$	denotes time derivative
$\hat{\ }$	denotes perturbation quantities
–1	matrix inverse or pseudoinverse

Sign Conventions

Angle of sideslip	Positive nose left
Differential flap	Positive right trailing-edge down (right-left)/2.0
Lateral acceleration	Positive out right wing
Lateral stick	Positive right roll
Roll rate	Positive right wing down
Rudder surface	Positive trailing-edge left
Yaw rate	Positive nose right
Yaw thrust vector command	Positive nose left

BACKGROUND

The X-31A program provided an opportunity to fly a quasi-tailless investigation. The availability of the aircraft and program resources allowed for an effective demonstration with a minimum of overhead cost.

Program Description

The experimental X-31A airplane was designed for enhanced fighter maneuverability (EFM) especially in the slow-speed flight environment (fig. 1). Two X-31A aircraft were built by Rockwell International (RI), Downey, California, and Daimler-Benz Aerospace (DASA), Germany, using joint funding from the Advanced Research Projects Agency (ARPA) and German Federal Ministry of Defense (FMOD). The initial program goals were rapid demonstration of EFM technologies, investigation of EFM tactical exchange ratios, development of design requirements and a database for future fighter aircraft, and development and validation of low-cost prototype concepts.

Under the auspices of the International Test Organization, which is composed of representatives from ARPA, FMOD, DASA, RI, United States Navy (USN), United States Air Force (USAF), and National Aeronautics and Space Administration (NASA), poststall envelope expansion and close-in-combat (CIC) evaluations were performed at the NASA Dryden Flight Research Center, Edwards, California. This flight test program successfully demonstrated the ability of the airplane to stabilize and maneuver in a controlled fashion up to 70° angle of attack (AOA) (refs. 3-5).

Upon completion of the initial program goals, an investigation was undertaken to demonstrate the ability of the thrust vector system to replace some or all of the functions of a vertical tail. The Joint Advanced Strike Technology (JAST) program funded a portion of the quasi-tailless flight test experiment.

Figure 1. The X-31A in poststall flight.

Aircraft Description

The X-31A airplane is a single-seat fighter configuration with a takeoff gross weight of approximately 16,000 lb. A single GE-F404 engine (General Electric, Lynn, Massachusetts) with an uninstalled gross thrust of approximately 16,000 lb at sea level powers this airplane. The planform includes a delta wing and a relatively small canard (fig. 2). The wing area, span, and mean aerodynamic chord are 226.3 ft^2, 22.8 ft, and 12.4 ft, respectively. The length is approximately 43.3 ft.

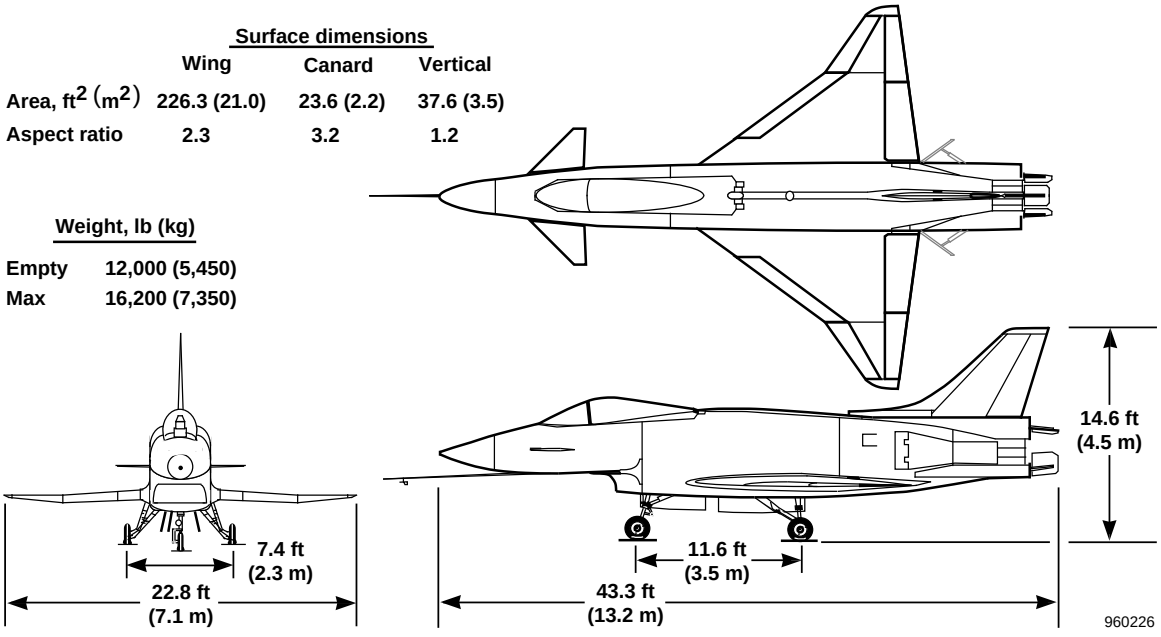

Figure 2. The X-31A planview.

The increased maneuverability of the X-31A airplane is obtained by using a thrust vector system to augment the control power provided by conventional aerodynamic control surfaces. The digital flight control system (ref. 6) uses a blended combination of aerodynamic and thrust vector control which depends on flight condition and thrust available.

Thrust Vector System Description

The thrust vector system provides pitch and yaw forces by deflecting paddles into the engine exhaust plume. Three carbon-carbon composite paddles are placed symmetrically around the engine nozzle (fig. 3). These paddles can be deflected a maximum of 35° into the plume. This paddle deflection range allows for maximum thrust vector deflection angles of approximately 15° for the majority of the engine power settings.

When no vectoring was required, the X-31A control laws positioned the paddles on the engine exhaust plume boundary. Such positioning ensured that when the paddles were deflected they would have an immediate effect. If the paddles were positioned outside the plume boundary, a lag would be introduced because the initial motion would be ineffective. The plume boundary position was calculated as a function of engine nozzle exit area and engine pressure ratio.

When a thrust vector command is issued, the amount of paddle deflection required is inversely proportional to the thrust available. For low-power settings, higher deflection angles are required to generate equivalent moments. The X-31A control system used a thrust estimation algorithm to determine the amount of deflection (gain) required of the thrust vector control loop. The thrust was estimated as a function of engine nozzle exit area, power lever angle (PLA), and engine pressure ratio. In simple terms, the thrust estimation algorithm approximates thrust by multiplying a pressure differential times an area. Accurate estimation of thrust is important for properly setting the gain on the thrust vector control loop. System stability can be adversely affected when, for example, the thrust is overestimated, so the control surfaces do not move enough. If the thrust is underestimated the paddles are commanded to move too far, which can also make the system unstable or generate undesired dynamics. The thrust estimation output

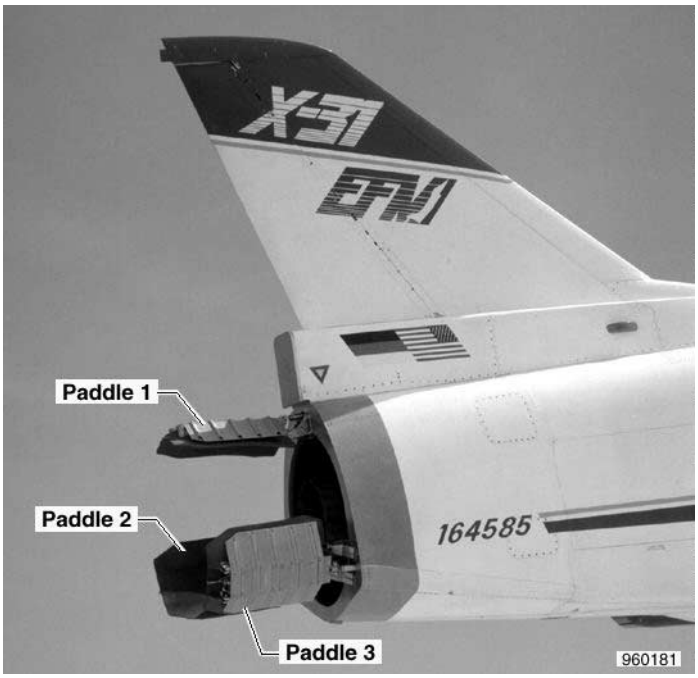

Figure 3. The X-31A thrust vector paddle arrangement.

was filtered to remove the noise associated with the algorithm input measurements and to smooth transitions caused by possible step failures of the simplex inputs to the algorithm. This filtering process introduces errors which have a direct effect on the thrust vector system loop gain.

Each thrust vector paddle command was rate limited in software to 60 deg/sec. The actuators were capable of up to 80 deg/sec; however, they were limited to reduce overall hydraulic demand in the case when all control surfaces were moved simultaneously. The ratio between paddle deflection and resulting thrust plume deflection is approximately 1.5 to 1.0. This ratio results in an effective thrust vector deflection rate limit of approximately 40 deg/sec. The nominal plume deflection range is up to 15°; however, the physical paddle deflection limitation of 35° results in a thrust vector deflection angle limit of less than 15° for some low-power conditions with small nozzle exhaust exit areas. In addition, collision could occur if any two paddles were deflected more than 26° simultaneously. Software limitations were imposed to avoid such collisions.

Incorporating thrust vectoring into flight control system requires a significant level of complexity. With a production axisymmetric nozzle, the plume boundary calculations and paddle collision avoidance logic are eliminated. On the other hand, the thrust estimation algorithm is still required, and limitations could be imposed because of airframe loads concerns.

Simulation Description

The X-31A program relied on a variety of simulations to assess flight safety and to plan and rehearse flight tests. The high-fidelity simulations included six-degree-of-freedom nonlinear equations of motion, a full-envelope aerodynamic database, the flight control computer hardware and software, the hardware actuator models, and a pilot cockpit and instrumentation panel (ref. 7). An example of one of the simpler simulations would be a fourth-order, linear model of the lateral–directional equations of motion. This paper describes results obtained from three simulations: a nonlinear FORTRAN batch simulation, a forth-order linear model, and a sixth-order linear model.

The nonlinear simulation discussed herein is an all FORTRAN six-degree-of-freedom batch simulation. A full-envelope aerodynamic database derived from wind-tunnel measurements, control laws recorded in FORTRAN, actuator, sensor, and time delay models are included. Pilot commands recorded from flight can be used as inputs to drive this simulation. Results from the nonlinear simulation can be compared directly to flight test measurements. The nonlinear simulation trim routines allow the simulation to be initiated in 1-g level flight, elevated load factor turns, or poststall. The simulation also includes a linearization function which uses numerical perturbations to calculate state-space rigid body equations of motion.

Fourth-order linear models derived from the nonlinear simulation (using the linearization function) were used to design the destabilization gains for the quasi-tailless control laws. These fourth-order, lateral–directional models included the roll, spiral, and dutch roll modes of the airframe at a particular trimmed flight condition. These models were used in open-loop simulation for gain calculations and in a closed-loop simulation to compare with flight test results. The closed-loop, fourth-order simulations included the destabilizing, restabilizing, and stability augmentation gains and feedback structure as well as pilot command gains.

For the X-31A airplane, the angle-of-sideslip feedback is a blended combination of noseboom sideslip vane and inertially derived angle of sideslip (fig. 4). The computational and transport delays in the inertial measurement values result in an equivalent time delay of approximately 67 msec in the sideslip feedback path. A sixth-order linear model was developed to include the effects of the delays on angle of sideslip. This model augmented the fourth-order model with a second-order model of the 67 msec time delay in the sideslip feedback path. The significance of this time delay is presented in the Results and Discussion section.

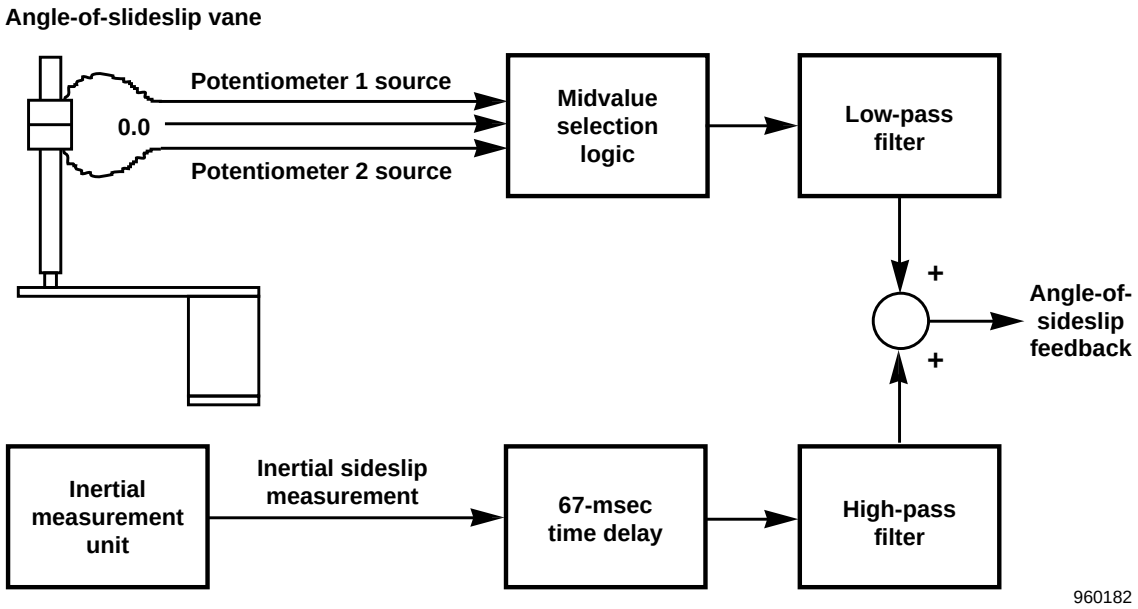

Figure 4. Sideslip feedback measurement system.

Flight Test Method

A flight test approach was developed which used the X-31A airplane to provide an initial look at the issues related to replacing the functions of a vertical tail and rudder surface with a thrust vectoring control device.

Concept

The quasi-tailless concept is to simulate a tailless or reduced tail airplane by using the rudder control surface to cancel the stabilizing effects of the vertical tail (refs. 8-10). The airplane is then restabilized and controlled by yaw commands to the thrust vector system. By using appropriate destabilization gains, various levels of directional stability can be simulated in flight without actually having to reduce the size of the vertical tail.

Figure 5 shows a simplified block diagram of the X-31A quasi-tailless control structure. (See also reference 10.) State-space linear perturbation rigid body equations of motion of the X-31A airplane without a vertical tail were formulated from wind-tunnel test data. Those models were in the following form:

$$\dot{\hat{x}} = A_{tailless}\hat{x} + B\hat{u}_{tailless}$$

where $\hat{x}$, the state vector is defined as

$$\hat{x} = \begin{bmatrix} \hat{\beta} \\ \hat{p} \\ \hat{r} \\ \hat{\phi} \end{bmatrix}$$

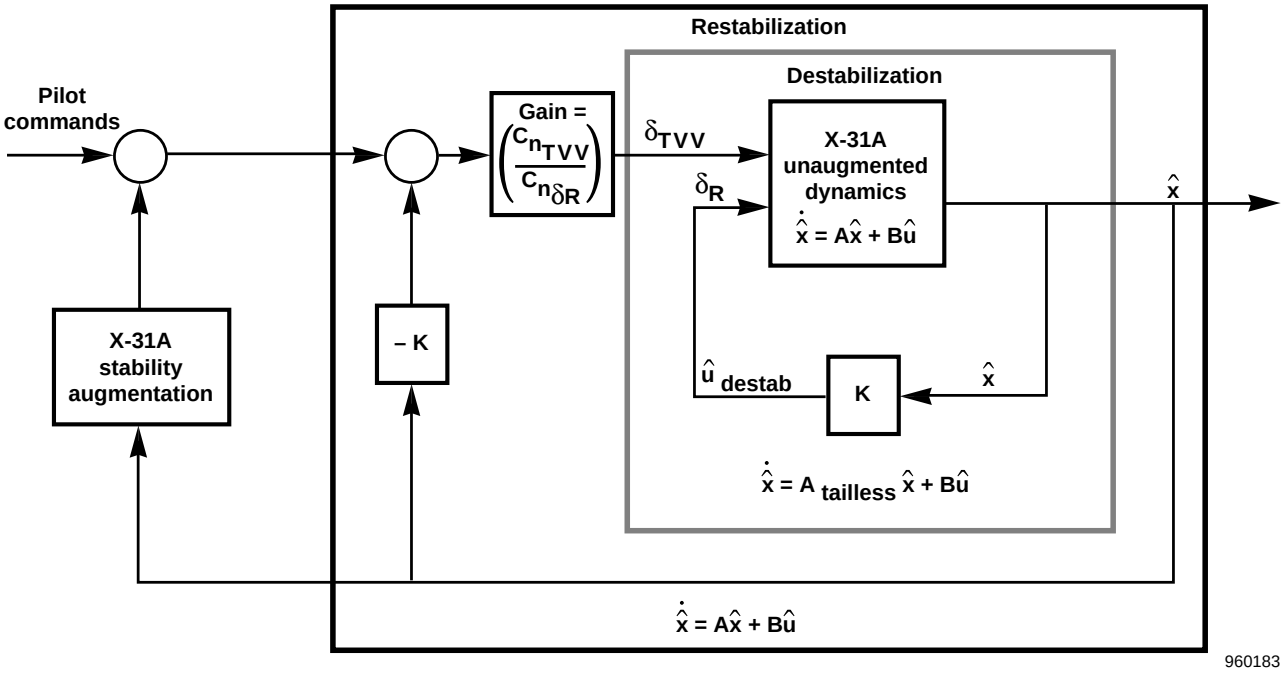

Figure 5. Simplified block diagram of quasi-tailless concept.

$A_{tailless}$ is the state derivative matrix for a tailless vehicle. It was assumed that the removal of the tail did not affect the control derivative matrix *B*. In reality, the aileron effectiveness would be slightly changed with the removal of a vertical tail. The vector $\hat{u}_{tailless}$ contains the control effectors available to a tailless vehicle; that is,

$$\hat{u}_{tailless} = \begin{bmatrix} \hat{\delta}_{df} \\ 0.0 \\ \hat{\delta}_{TVV} \end{bmatrix}$$

Similarly, for an X-31A airplane with a tail but without thrust vectoring, the state-space model was defined as follows:

$$\dot{\hat{x}} = A\hat{x} + B\hat{u}$$

Here, the control vector $\hat{u}$ contains control effectors available for a conventional tailed vehicle; that is,

$$\hat{u} = \begin{bmatrix} \hat{\delta}_{df} \\ \hat{\delta}_R \\ 0.0 \end{bmatrix}$$

A destabilizing feedback controller was used to transform the existing X-31A dynamics into simulated X-31A tailless dynamics.

$$\dot{\hat{x}} = A\hat{x} + B\hat{u} + B\hat{u}_{destab}$$

where

$$\hat{u}_{destab} = K\hat{x}$$

which gives

$$\dot{\hat{x}} = (A + BK)\hat{x} + B\hat{u}$$

To match the tailless dynamics, the following must be true:

$$(A + BK) = A_{tailless}$$

or

$$K = B^{-1}(A_{tailless} - A)$$

The simulated tailless system was restabilized using the thrust vector system. The destabilizing effects from the rudder were canceled by changing the sign of the rudder command, scaling it by the ratio of control effectiveness derivatives $(c_{n_{TVV}}/c_{n_{\delta R}})$, and sending this command to the thrust vector system (fig. 5). The thrust vector system also replaced the rudder for turn coordination and handling qualities augmentation.

Different levels of tail removal can be simulated simply by replacing $A_{tailless}$ in the gain calculation, *K*, with a suitable state-space representation of a vehicle with a partial tail. This quasi-tailless system provides a method for assessing the control power usage required for various levels of destabilization.

If the thrust vector system matches the bandwidth and control power of the rudder surface, then any destabilizing feedbacks will be exactly canceled (fig. 5). Figure 6 shows that the actuator dynamics derived from ground test compare well for the thrust vector system and the rudder. Below 100 rad/sec, the maximum difference in gain is less than 0.5 dB and in phase less than 4°.

Implementation

Using fourth-order linear models, the destabilizing control law gains were calculated for a full tailless vehicle at a given flight condition. For the X-31A quasi-tailless experiment, the bank angle, ϕ, feedback gain magnitudes were low enough to neglect. Multiplying the feedback gains by a scale factor which varies from 0.0 to 1.0 results in a destabilization level from no tail reduction to 100-percent tail reduction. Using a control system interface console, the pilot selected gains for discrete levels of tail reduction. For 0-percent tail reduction the quasi-tailless control laws provided no destabilizing feedback to the rudder surface; however, the stability augmentation and roll coordination yaw commands were diverted from the rudder to the thrust vector vane system. Thus, selecting 0-percent tail reduction resulted in a fixed rudder control surface with the thrust vector vane system providing any required turn coordination or stability augmentation. The 0-percent tail reduction setting is equivalent to setting the control law gain, *K*, of figure 5 to 0.0.

The initial quasi-tailless flight tests included a “destabilized-only” quasi-tailless mode. In this mode, the destabilizing commands to the rudder were allowed; however, the restabilization and stability augmentation commands to the thrust vector system were disabled. This mode was incorporated to validate the destabilization process. Pilot selection in the destabilize-only mode was limited to tail reduction settings which resulted in neutral to slightly unstable vehicle dynamics. High levels of destabilization were precluded by software.

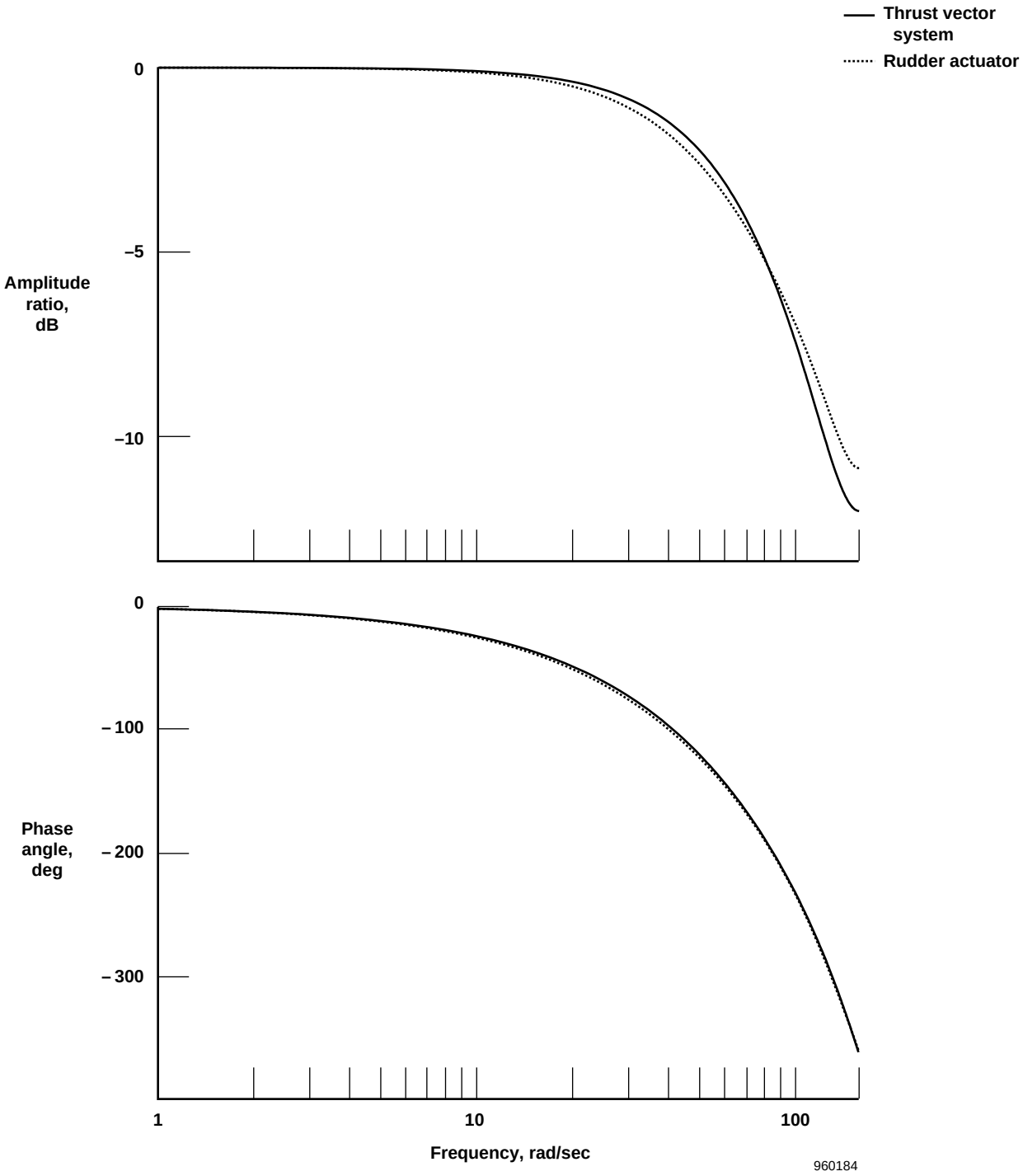

Figure 6. Comparison of thrust vector and rudder actuator frequency response.

For safety reasons, disengagement of the quasi-tailless mode was automatically initiated upon violation of a number of flight condition and vehicle state requirements (table 1). Upon disengagement, the rudder and thrust vectoring system resumed their stability augmentation roles. A mechanical throttle stop was installed in the airplane to avoid quasi-tailless mode disengagements caused by reducing the power lever angle (PLA) below the lower limit.

Nonlinear simulation showed that the amount of instability that could be controlled by thrust vectoring was determined by the level of roll acceleration and roll rate required. The X-31A airplane was developed to demonstrate high levels of agility. As a result, its maximum commanded roll rate and roll acceleration were high (up to 240 deg/sec and 610 deg/sec^2). With these high rates and accelerations, initiation of rolls demanded more coordinating yaw control power than was available from the thrust vector system at low-power settings. The subsonic quasi-tailless control law design attempted to tailor the roll command to that which could be controlled by the thrust vector system at a setting of 50- to 60-percent tail size reduction. The maximum commanded roll rate was reduced by as much as 50 percent for low-power settings. Meanwhile, the roll acceleration command limit was reduced by as much as 65 percent to match the amount of thrust vectoring yaw control power available at low-power settings. The maximum roll acceleration command limit was scheduled as a function of power setting.

Flight Test Plan

Quasi-tailless flight testing was accomplished in two phases with two software loads. The first testing phase was a limited demonstration of the concept at a single point design. The design point was an altitude of 38,000 ft at Mach 1.20. This flight condition represents a supersonic cruise condition where a reduction in tail size results in a large drag savings. The maneuvers flown at the supersonic test point consisted of roll and yaw doublets, 30° bank-to-bank rolls, and gentle wind-up turns to 2 *g*. These maneuvers were flown with high engine power settings. Table 1 shows the disengagement criteria imposed on the quasi-tailless mode for the supersonic flight condition.

Table 1. Quasi-tailless mode safety disengagement criteria.

	Supersonic limits		Subsonic limits	
Parameter	Lower	Upper	Lower	Upper
Angle of sideslip, deg	–1.5	1.5	---*	---*
Angle of attack, deg	0.0	10.0	0.0	20.0
Power lever angle, deg	100.0	---	55/65†	103/132†
Mach number	1.10	1.30	---	---
Altitude, ft	30,000	40,000	---	---

*Function of dynamic pressure, approximately ±10.0 at 170 KIAS, ±2.6 at 400 KIAS.
†Gear down values/gear up values.

The second flight test phase extended the quasi-tailless testing to a larger subsonic flight envelope. To support JAST requirements, two tasks were selected to demonstrate operability of a tailless or reduced tail vehicle: a simulated carrier approach landing task and a ground attack profile. Maneuvers flown to clear the airplane for these tasks included roll-yaw doublets, full stick bank-to-bank turns, steady heading sideslips, and 360° rolls. Testing was accomplished with changes in power settings, speed brakes, and landing gear status. The safety disengagement criteria were relaxed to allow for a larger maneuvering flight envelope (table 1).

The precision approach task was to line up on and maintain a precise flightpath as if on approach to a carrier landing. Deviations from the desired flightpath were corrected for by aggressive pilot inputs to the longitudinal and lateral stick and to the throttle. To provide feedback cues to the pilot, an angle-of-attack indexer was added to the cockpit instrumentation system, and a Fresnel lens landing system was temporarily installed on one of the runways at Edwards Air Force Base, California (ref. 9). These landing aides provided the pilot with cues for tight control of angle of attack (approach speed) and flightpath angle.

A nominal flightpath angle of 2.5° was chosen. The airplane was configured with the landing gear down and speed brakes out. The desired task performance criteria were to maintain glide slope within ± 0.5 ball with respect to the Fresnel lens (± 0.17°), heading within ± 1°, and angle of attack within ± 0.5°. For adequate performance, ± 1 ball (± 0.34°) glide slope, ± 2° heading, and ± 1° angle of attack were required. Approaches were flown to a waveoff at 100 ft above ground level (AGL) because the X-31A landing gear was not designed for the high loads required of a carrier approach touch down.

A more challenging lateral task was introduced by initial lineups of one-half runway width (approximately 40 ft) to the left or right of the runway. Corrections to this offset were applied either at the start of the approach (1.5 n.mi. distant or 400 ft AGL) or in the middle of the approach (1.0 n.mi. distant or 270 ft AGL).

Flight test evaluations of three simulated ground attack profiles were also performed (fig. 7). The first profile included a pop-up and climb followed by a roll-in and pull-down maneuver for a rapid gross acquisition of a ground target. When the target was acquired, the pilot was required to rollout to wings level and set up a 15° glide slope bomb run while tracking the ground target. The desired task performance criterion for gross acquisition was to obtain the target within a 40-mrad reticle with no overshoots; adequate performance was achieved with one overshoot. Fine tracking desired criterion was to maintain the target within a 20-mrad reticle with no overshoots, and adequate performance was achieved with one overshoot. Task performance criteria were the same for all ground attack profiles.

Figure 7 shows the second ground attack profile which consisted of a 15° glide slope bomb run using the Adaptable Target Lighting Array System (ATLAS) for the ground target (ref. 11). This ground attack run was flown without the pop-up portion of the profile. This attack was initiated from an altitude of 4000 ft AGL and 400 KIAS. The X-31A airplane would then execute a 4-*g* turn to acquire the ATLAS ground target. The ATLAS consists of an array of target lights positioned on the ground. A fine tracking task is created by randomly sequencing the target lights and requiring the pilot to acquire each light with the gun reticle. Upon completion of the light sequence, a pull-out maneuver was performed followed by evasive maneuvering.

The third ground attack profile consisted of a high-altitude approach to a 45° glide slope run (fig. 7). Again, the pop-up portion of the profile was deleted. Instead, the roll-in maneuver was initiated from level flight at 18,000 ft AGL to a 45° glide slope. For this profile, ATLAS was not used because it is set up for a lower glide slope approach. A preselected ground feature, such as a water tower, Joshua tree, or road intersection, was used for the acquisition and tracking target. Reference 9 provides a detailed description of the ground attack profiles.

RESULTS AND DISCUSSION

This section describes the results obtained from the supersonic and the subsonic flight tests.

Supersonic Test Results

The supersonic testing provided an initial demonstration of the quasi-tailless concept and showed maneuvering capabilities consistent with those required of a supersonic transport airplane. The destabilized-only mode was flown up to a selection of 20-percent tail reduction. The pilot commented, “the 20-percent destabilized cases clearly

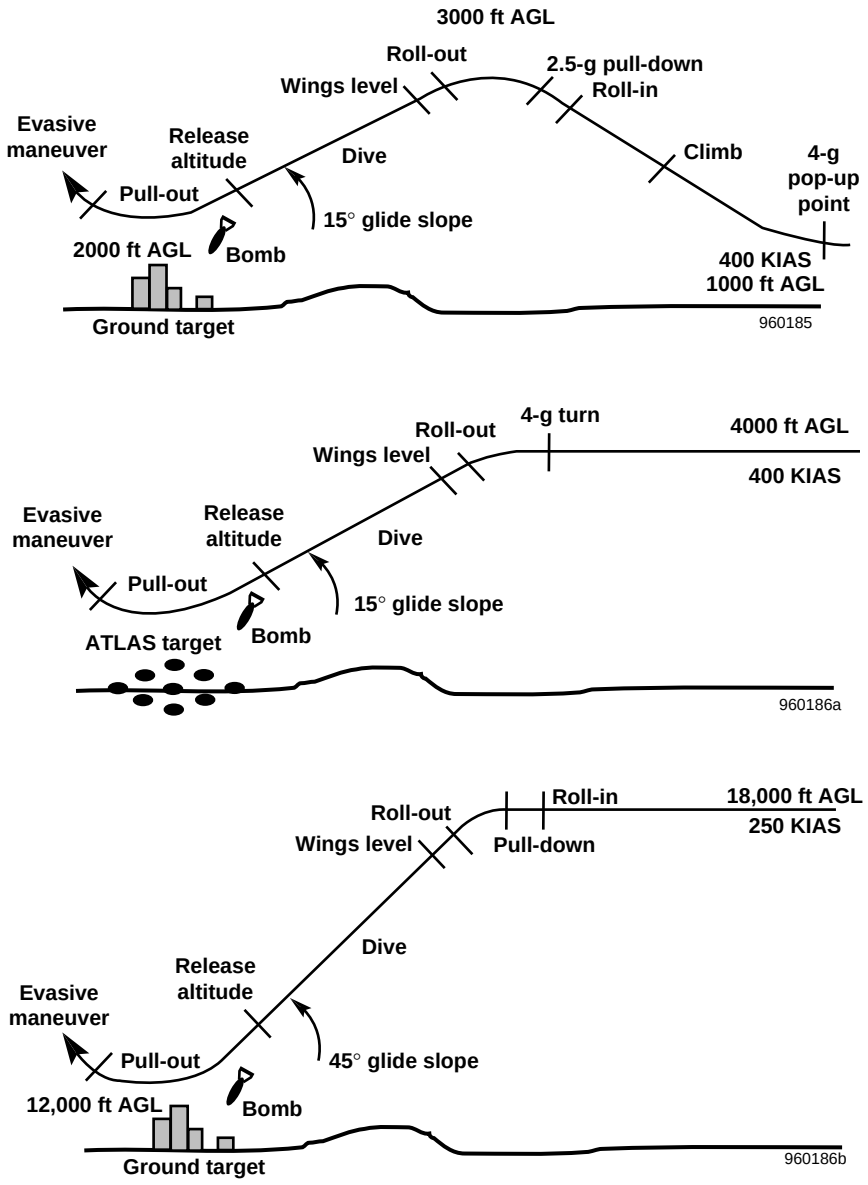

Figure 7. Air-to-ground flight profiles.

showed reduced directional damping with several overshoots observed." The full quasi-tailless mode with the thrust vector system engaged for restabilization was flown to a maximum setting of 70-percent tail reduction (approximately 170-msec time-to-double amplitude). The pilot said, "the aircraft response was satisfactory for all [tested] values of tail off."

A one-half stick roll doublet was performed at an altitude of 38,000 ft and Mach 1.20. A comparison of flight and nonlinear simulation showed a good match for the 20-percent destabilization-only case (fig. 8). The match between flight and a fourth-order linear model shows a difference in the damping of the oscillations (fig. 9). This difference resulted from the filtering in the sideslip feedback loop. When a second-order approximation of this delay is added to the sideslip feedback, the resulting sixth-order linear model produces an improved match to the flight data (fig. 10).

With the delays in the sideslip feedback, the level of destabilization achieved in flight was less than that predicted by the simple fourth-order model. Consequently, the achieved level of destabilization differed from the

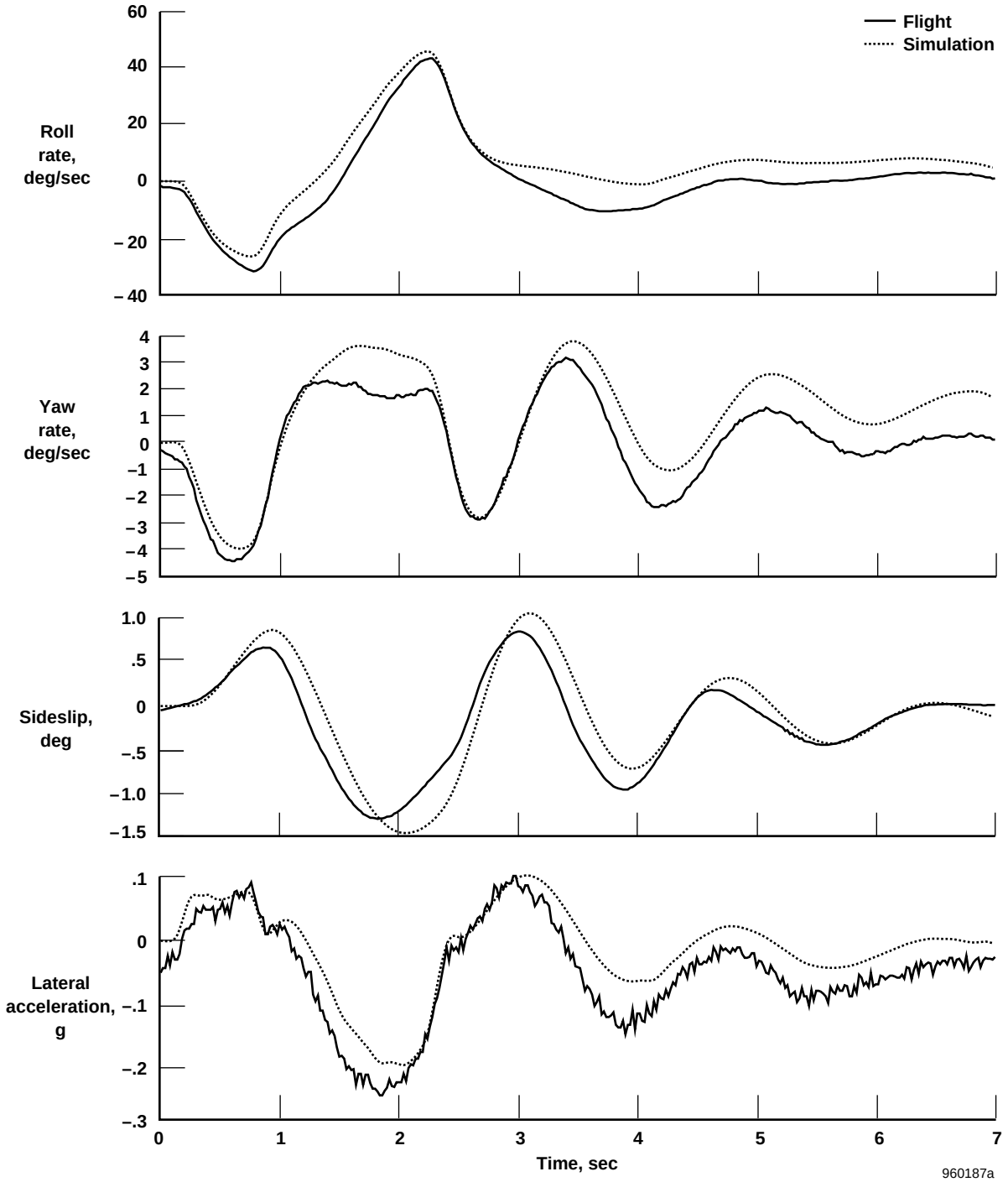

Figure 8. Roll doublet at Mach 1.2 in the 20-percent destabilize-only mode (comparison of flight data to a nonlinear simulation).

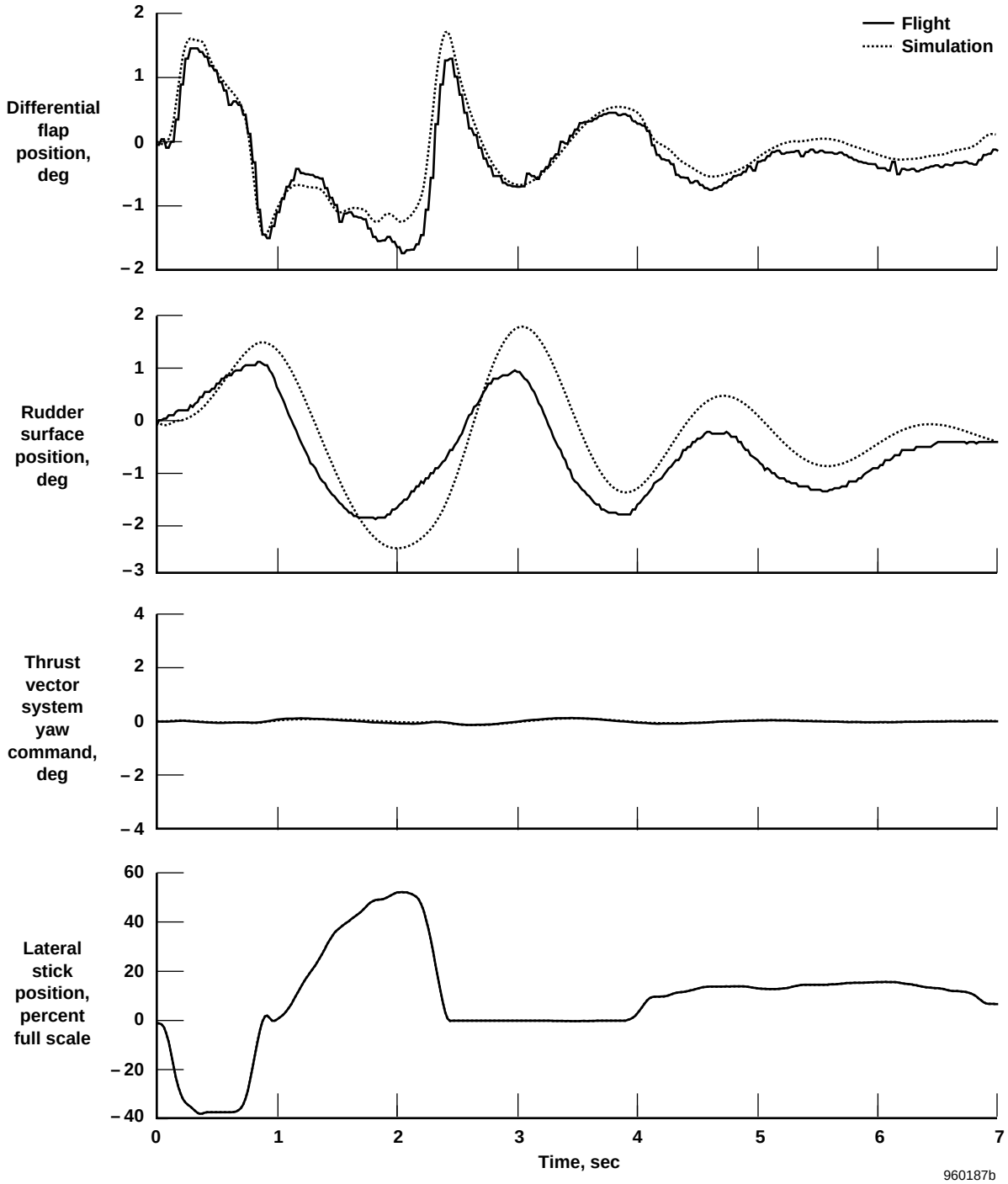

Figure 8. Concluded.

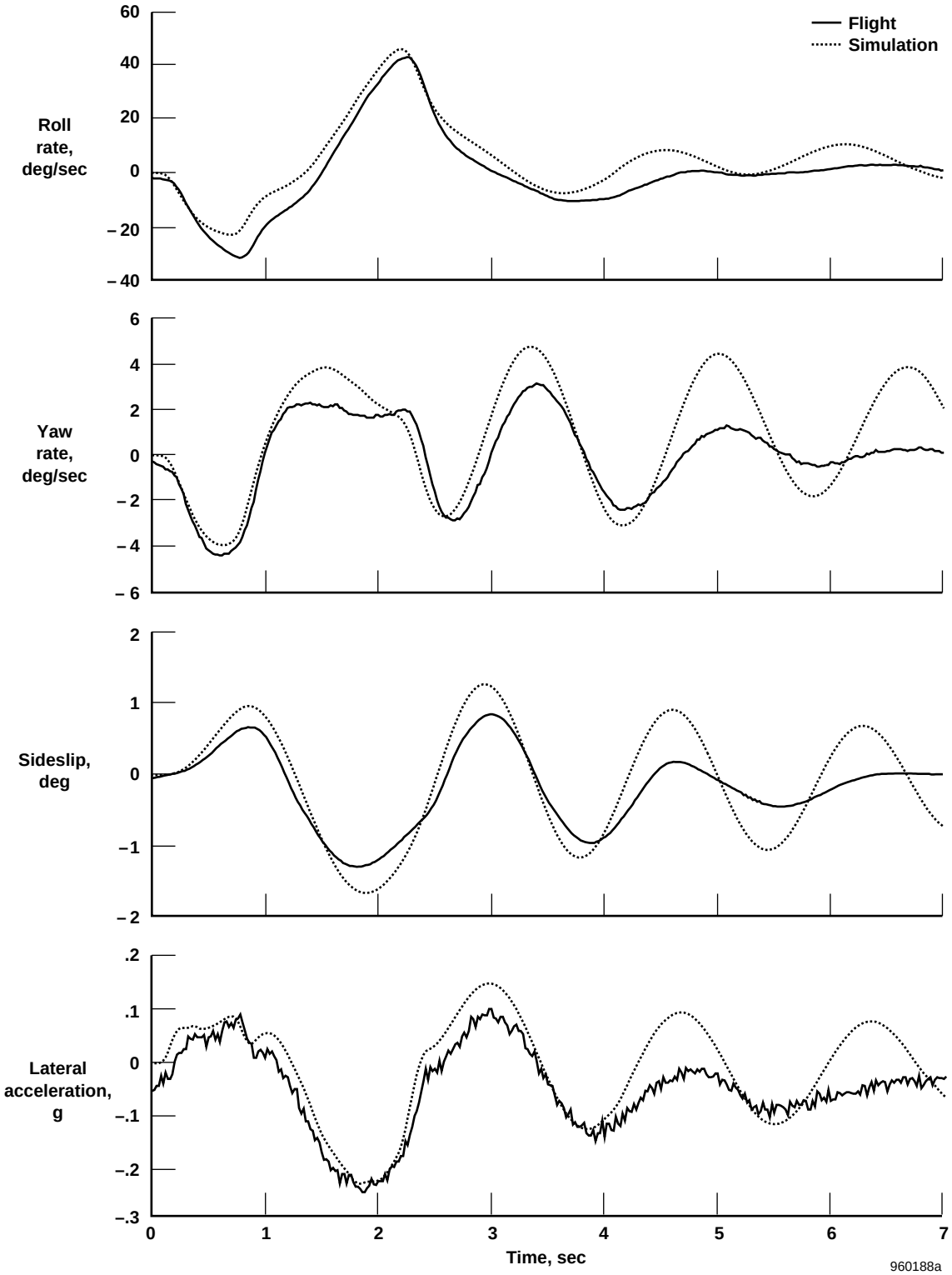

Figure 9. Roll doublet at Mach 1.2 in the 20-percent destabilize-only mode (comparison of flight data to a four-state linear model).

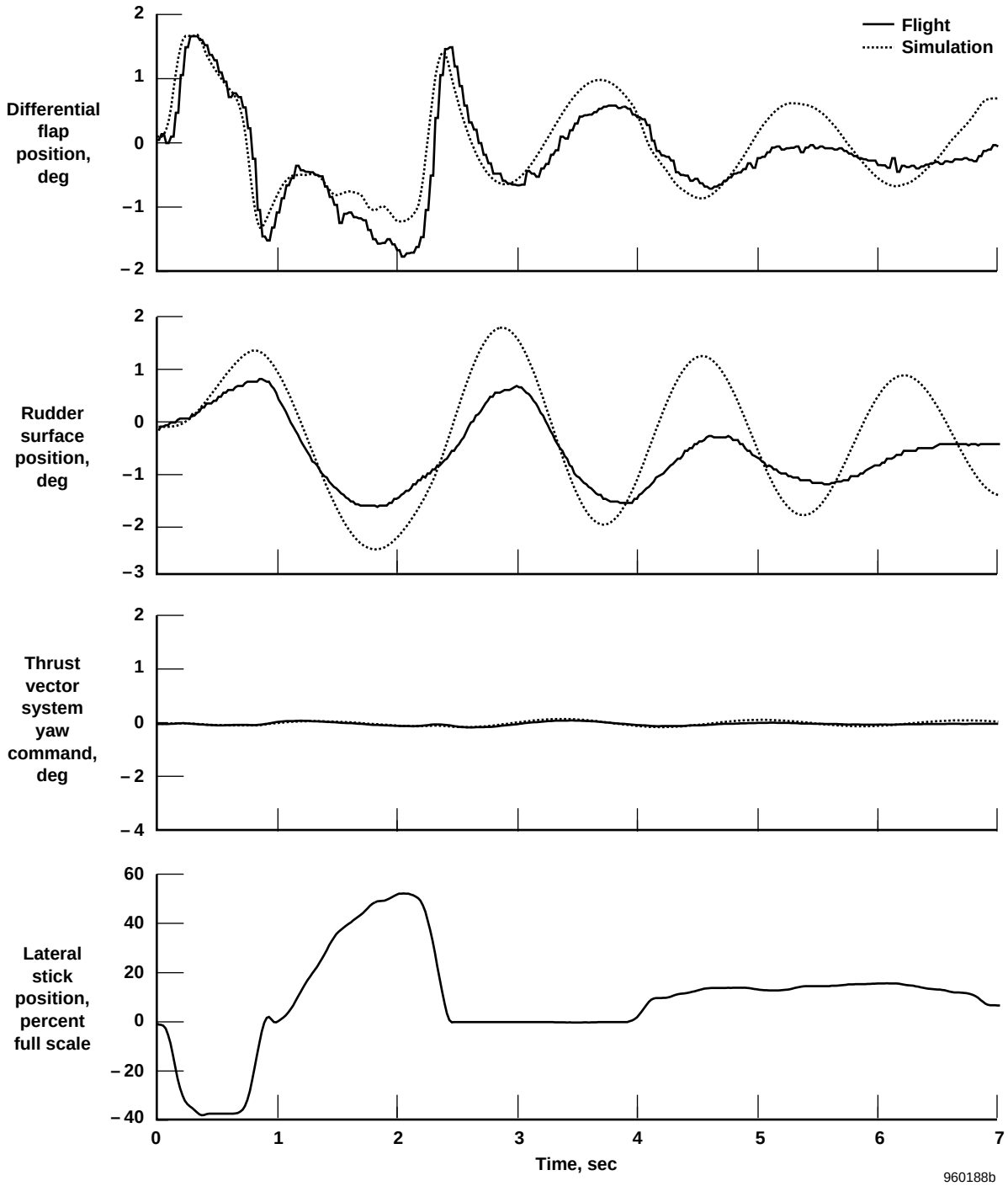

Figure 9. Concluded.

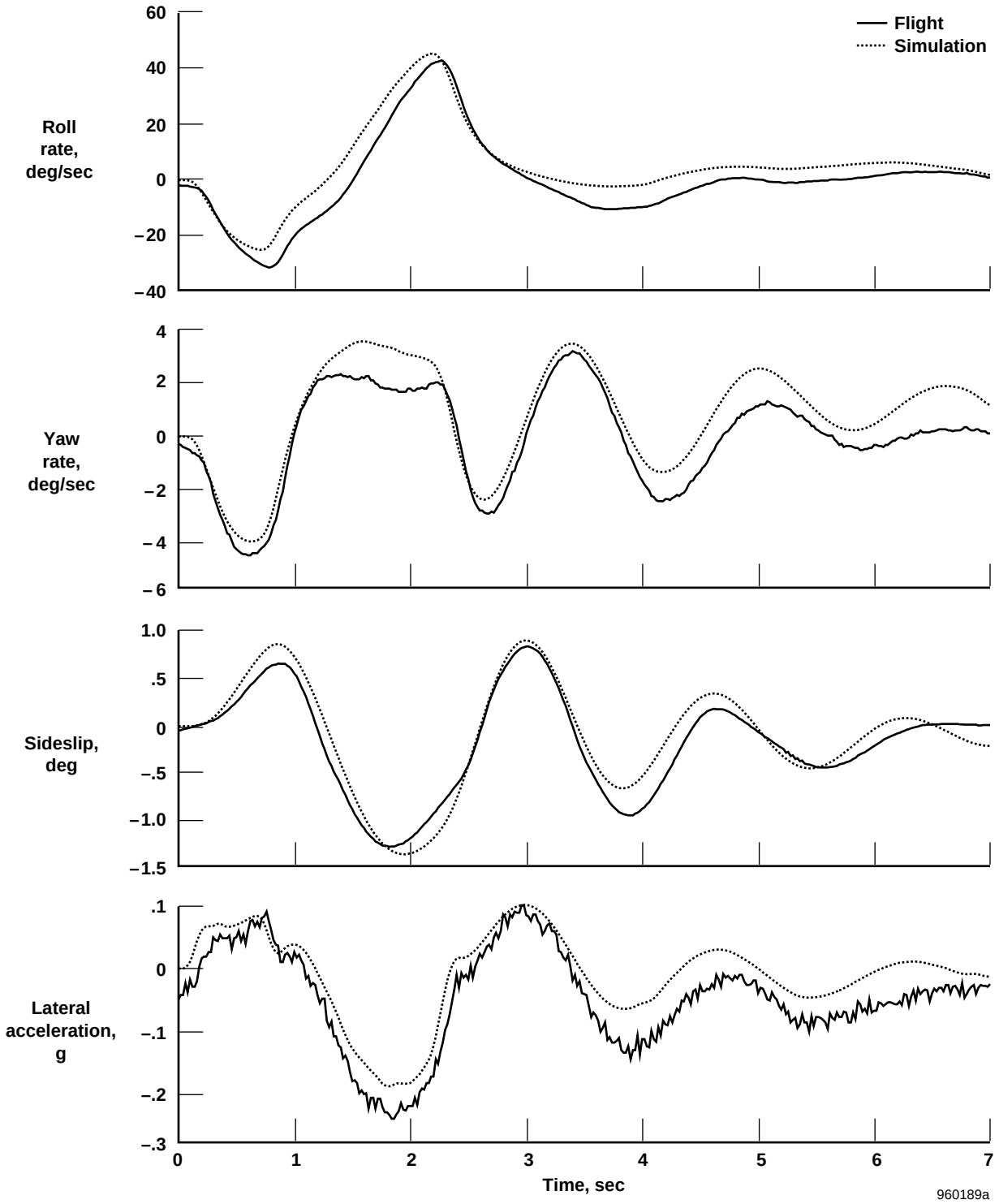

Figure 10. Roll doublet at Mach 1.2 in the 20-percent destabilize-only mode (comparison of flight data to a six-state linear model).

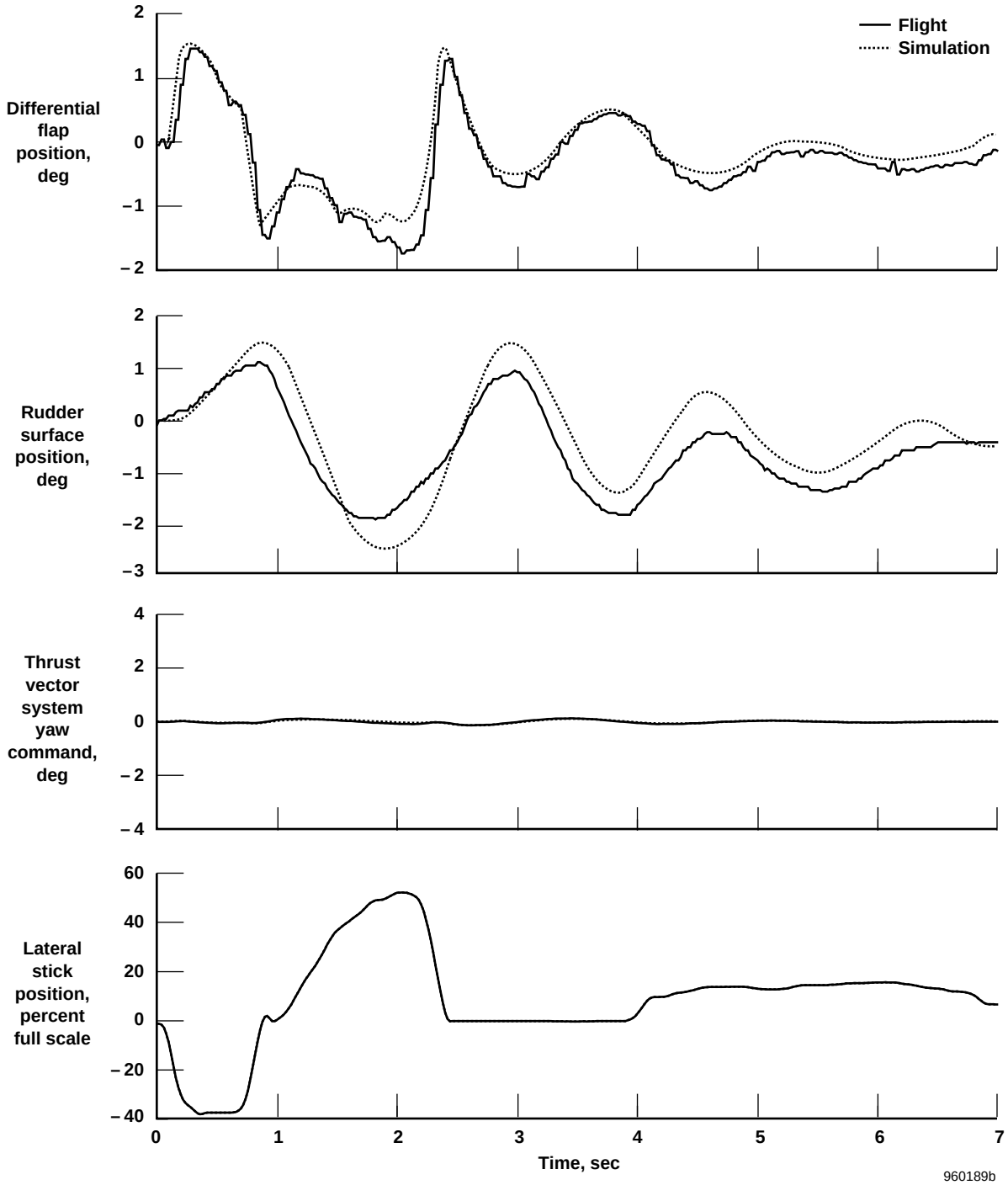

Figure 10. Concluded.

design goal. Figure 11 shows the root locations for the fourth-order linear model and a sixth-order model which incorporates an approximation of the 67-msec delay on the sideslip feedback path. The dutch roll damping is 0.1 for the sixth-order model and 0.03 for the fourth-order model. Adequately designing destabilization gains requires that delays on the angle-of-sideslip feedback path be considered.

Close scrutiny of the flight data uncovered another undesirable characteristic in the sideslip feedback path. The vane-sensing logic was creating a deadband effect on the measured sideslip angle. To understand how the deadband was created, the redundancy management logic for the sideslip feedback must be described. The angle of sideslip is measured by two potentiometers mounted to a single sideslip vane. For redundancy and to maintain consistency with logic used for triplex signals, three signals were sent to the selection logic: the two potentiometers and a constant value of zero. Then, a middle value selection logic scheme was used to chose the feedback quantity used by the flight control computers (fig. 4). This type of logic protects against a hard-over failure of an electrical signal. In the presence of a hard-over failure, the middle value would be either zero or the unfailed signal. This selection logic also means that if the two electrical signals differ in sign, the selected middle value is a constant of zero.

These flight data indicate that a small bias existed on each electrical signal ($-0.25°$ and $0.15°$). Whenever the sideslip angle was between $-0.15°$ and $0.25°$, the selected value sent to the flight control computers was 0.0. Thus, the biases result in system operation with an effective deadband on the sideslip feedback of approximately $0.4°$ around a zero reading.

As figure 4 shows, the sideslip feedback quantity is a blended combination of the low-frequency components of the sideslip vanes and the high-frequency components of the inertial measurement system. This combination means that the steady-state reading of zero was passed through into the control system. Normally a small deadband on sideslip would not be very noticeable; however, the high gain destabilizing feedbacks used in the quasi-tailless experiment accentuated this effect. The deadband was noted in the data of the supersonic and the precision approach testing.

Midway through the program, failure of the sideslip vane potentiometer forced a replacement of the noseboom assembly. Subsequent testing during the ground attack flight demonstrations indicated that the deadband had been

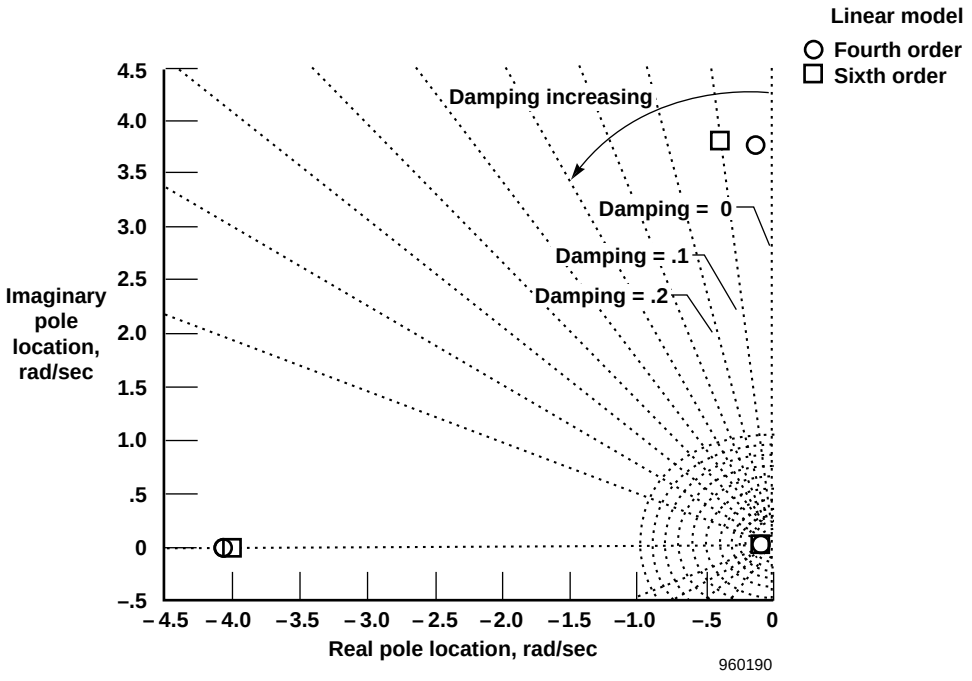

Figure 11. Effect of sideslip feedback lag on closed-loop poles.

virtually eliminated with the new noseboom. As a result, the supersonic and precision approach tests were affected by the deadband, and the ground attack tests were not.

The 20-percent, destabilization-only case shown in figure 8 indicates that for a one-half stick input the size of the sideslip excursion was $\pm 1.0°$. This relatively loose sideslip behavior is a direct result of the reduced damping caused by the destabilization feedbacks. The biases on sideslip sources and middle value signal selection logic were included in the nonlinear simulation to assess their impact. For this magnitude of sideslip, the ratio between true sideslip and the inertially derived feedback quantity from simulation was approximately 0.90.

A simple model of the deadband affect could be achieved by incorporating a gain reduction in the sideslip feedback path of approximately 10 percent into the linear model. The linear model showed that a gain reduction of 10 percent had a minimal effect on closed-loop pole locations for this case.

Another one-half stick roll doublet was performed at an altitude of 38,000 ft and Mach 1.2, this time with a setting of 70-percent tail reduction. In this case, the full quasi-tailless mode was selected which means that the thrust vector system was used to restabilize the vehicle. The damping provided by the stability augmentation resulted in reduced sideslip excursions ($\pm 0.4°$) when compared to the destabilization-only mode. As a result, an increased amount of the maneuver occurred within the deadband. Thus, the deadband had a much more pronounced affect on the quasi-tailless mode than on the destabilization-only mode.

Figure 12 shows a comparison of flight data and the nonlinear simulation which includes a model of the deadband on the sideslip feedback. Output of the sideslip vane middle value selection logic was zero for the majority of the maneuver, and it never shows a positive reading. The inertially derived quantity, which is a blended combination of inertial measurement unit and sideslip vane measurements, seems to indicate that true angle of sideslip did have positive excursions. During roll inputs, the X-31A control laws actively minimize the amount of sideslip excursion. As a result, the size of the deadband is a large percentage of the size of the feedback signal.

The deadband was included in the nonlinear simulation. The ratio of true angle of sideslip and inertially derived angle of sideslip obtained from the modified nonlinear simulation was approximately 0.80. Thus for this case, the deadband was equivalent to a sideslip feedback loop gain reduction of approximately 20 percent. Closed-loop system behavior becomes a function of the size of the input; therefore, a linear model does not provide a good measure of the level of destabilization achieved.

Thus, the supersonic flight data revealed that the lag in the sideslip feedback path and the deadband in the vane-sensing system should be considered when assessing the results of the quasi-tailless study.

Subsonic Test Results

The second phase of quasi-tailless flight testing was performed with control law software which allowed for a large maneuvering flight envelope in the subsonic region. Precision landing approaches and ground attack tasks were flown. For the first time, thrust vectoring was used as a primary controller in conjunction with low-power settings.

Precision Approach Task

Designing control laws for the landing approach flight phase is critical for a tailless or reduced tail airplane. In this flight phase, the airplane is flown with reduced engine power settings and, consequently, has low thrust vectoring control power. In addition, the active throttle movements required to maintain a tight flightpath mean that the control power can change rapidly. This task is accomplished close to the ground where increased turbulence levels are also expected.

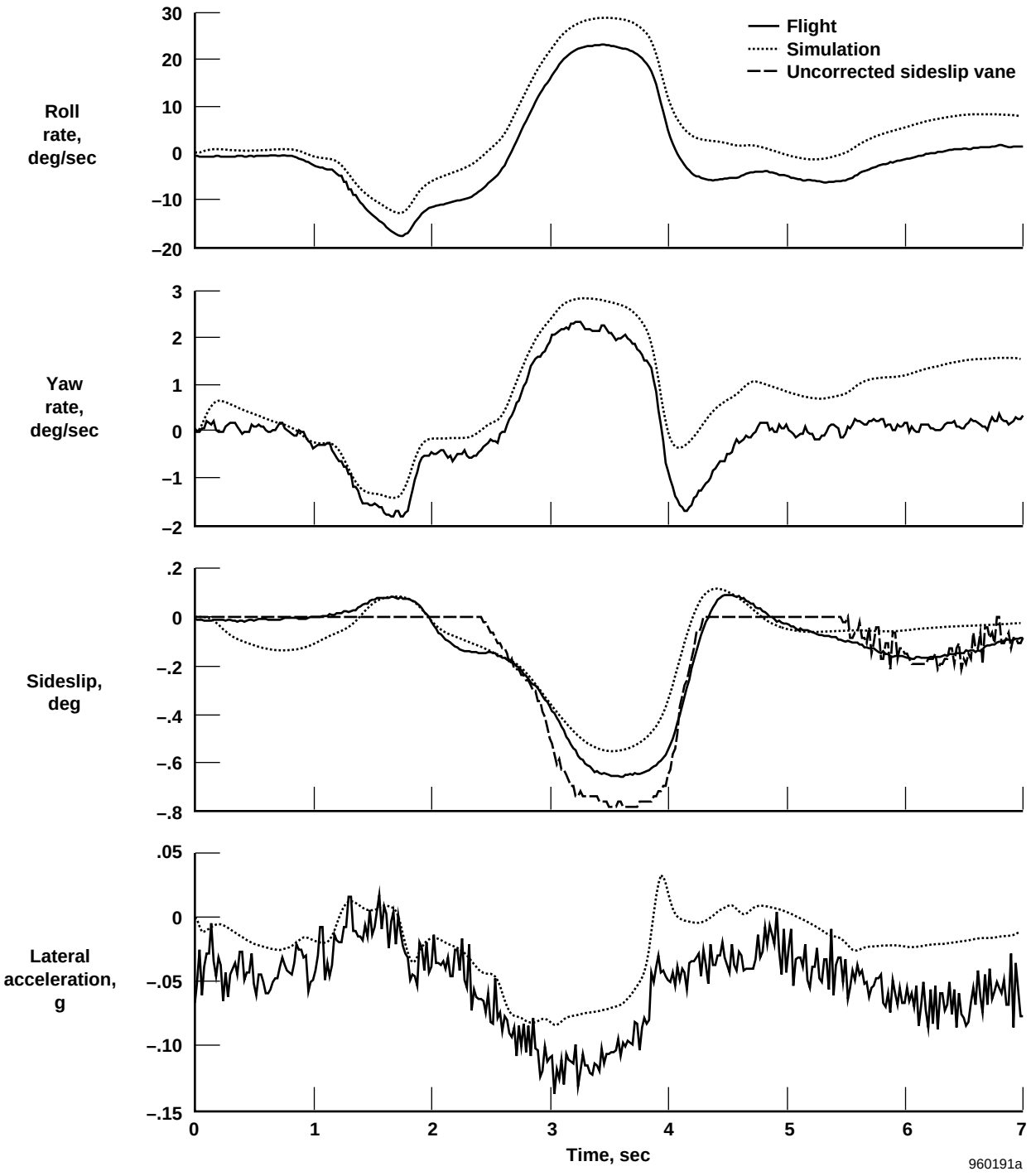

Figure 12. Roll doublet at Mach 1.2 in the 70-percent tail reduction setting (comparison of flight data to a nonlinear simulation).

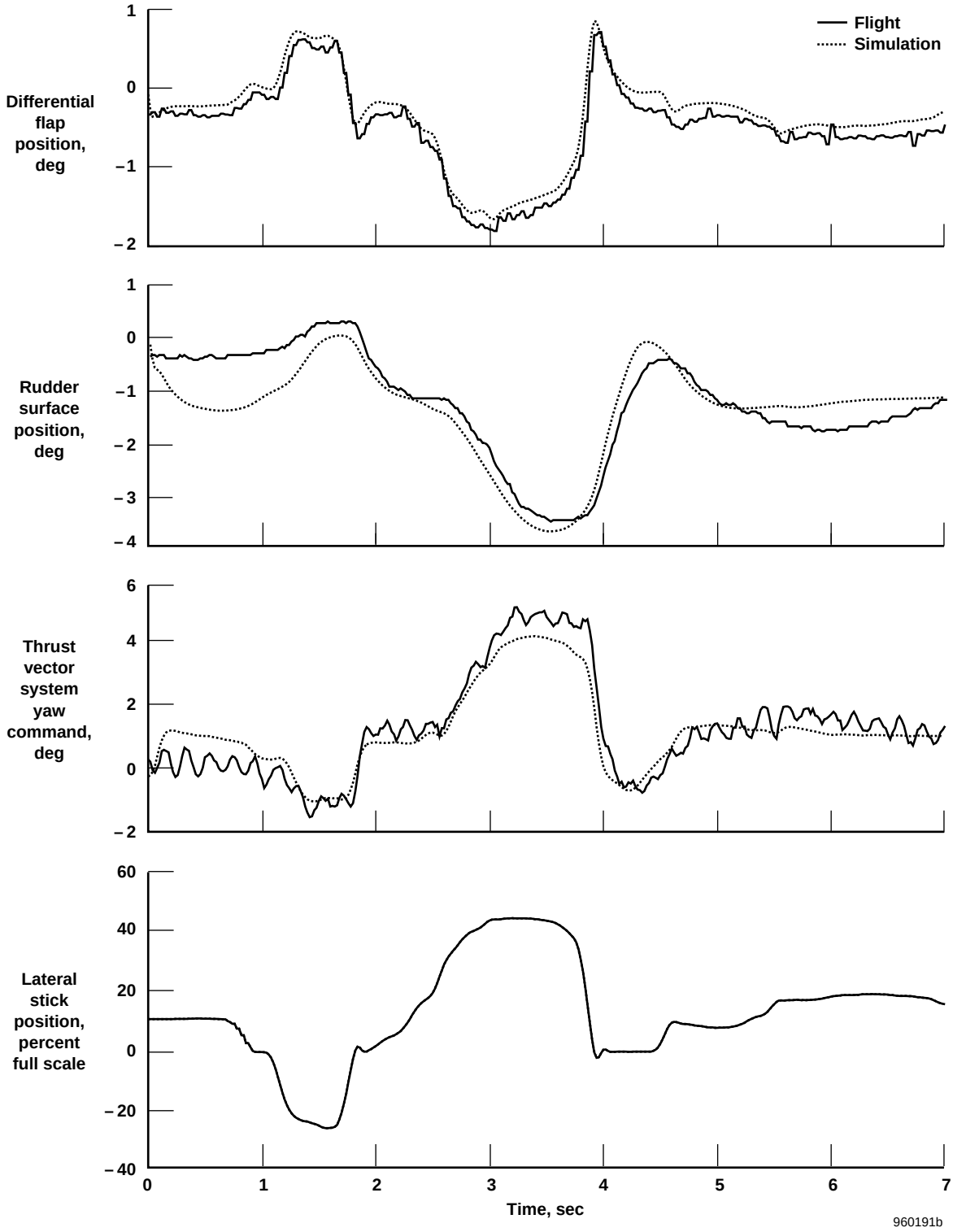

Figure 12. Concluded.

Two X-31A pilots flew 27 precision approaches on three flights. These approaches were flown with the baseline X-31A control laws and for quasi-tailless settings of 40- and 50-percent tail size reduction. Table 2 shows the pilot ratings obtained for these tests. The pilots noted there were “no perceptible change in flying qualities” caused by the quasi-tailless mode. As a result, the Cooper-Harper ratings (CHR) (ref. 12) for the precision approach task did not change with respect to the level of destabilization selected. Pilot inputs for the precision approach task were small and did not produce any rate or position saturation of the thrust vector paddles for the tail reduction settings that were flown.

Table 2. Precision approach pilot comments.

Flight number	Run	Lineup/ correction	Tail reduction setting, %	CHR	Comments
277	1	Right/start	Basic	5	Aircraft is responding well in roll, sensitive in pitch.
277	2	Nominal	Basic	5	Sensitive in longitudinal axis, more friction and breakout required. AOA hold in powered approach needs to be better, too much AOA variation.
277	3	Left/start	Basic	N/A	N/A
277	4	Left/middle	Basic	4	Corrections in the middle achieved proper gains. No dutch roll observed. Very stable aircraft.
277	5	Right/middle	Basic	4	Good roll rates and response. No adverse handling qualities observed.
277	6	Left/middle	Basic	5	Over control pitch, drove ball one cell high in close.
277	7	Right/middle	Basic	5	N/A
278	1	Nominal	Basic	N/A	*The flying qualities in quasi-tailless (40 and 50 percent) were the same as the basic airplane during the “carrier approaches.” In general, the roll axis had a better sensitivity in travel-force per roll rate than pitch. The pitch axis is more sensitive (too sensitive). The throttle is sensitive with small corrections for glide slope control. Throttle sensitivity tends to cause overcontrol of power. CHR's of 4-5 were due to difficulty in glide slope control. Lateral (line-up) was always a CHR 2. Did not see any aircraft movements due to throttle changes. Did have one disengagement as throttle was retarded below 56° PLA throttle stop. Line-up corrections at the start were easy with no overshoots or overcontrol. Line-up corrections in the middle required a more aggressive input. Aircraft response was excellent. Precise attitude control and line-up capture with no overshoots. This task in general is a CHR 2.
278	2	Nominal	40	5	
278	3	Nominal	50	4	
278	4	Left/start	Basic	4	
278	5	Right/start	40	4	
278	6	Left/start	50	4	
278	7	Right/middle	Basic	4	
278	8	Left/middle	40	3	
278	9	Right/middle	50	N/A	

*Summary of comments for the entire flight.

Table 2. Continued					
Flight number	Run	Lineup/ correction	Tail reduction setting, %	CHR	Comments
279	1	Nominal	Basic	5	Overcontrolled glide slope, sensitive in pitch, difficult to maintain AOA.
279	2	Nominal	40	4	Can not tell the difference versus basic thrust vector. AOA is still difficult to control, ball control was better, and *still a lot of compensation*. No dutch roll. Throttle response was good, did not feel the throttle stop. Test conductor said that PLA stayed above 60°.
279	3	Nominal	50	6	Exceeded desired criterion in close, drove the ball one cell high. Overcontrolled the long stick. *Lateral-directionally very stable.* AOA not under control.
279	4	Left/start	Basic	5	Drove the ball a cell high on the right for line-up call. In close, right on parameters. CHR 5 primarily for glide slope criterion.
279	5	Right/start	40	4	Disengaged for PLA just before wave-off.
279	6	Left/start	50	5	Disengaged for PLA on centerline capture. FQ were very good; no change in FQ on disengagement. No dutch roll. Throttle response was good.
279	7	Right/middle	50	4	High start. QT stayed engaged throughout. No adverse FQ noted on roll-out or centerline capture; lots of compensation required.
279	8	Nominal	Basic	4	Working pretty hard, *but not discerning any change in workload between 50 percent or basic*. CHR 4 for workload and compensation.
279	9	Right/middle	50	4	CHR for compensation required. No adverse FQ noted.
279	10	Left/middle	50	5	Overcontrolled glide slope in close and drove the ball one cell high.
279	11	Right/middle	50	4	On parameters, nice approach, QT working well. Still no perceptible change from basic aircraft.

The powered approach flight condition flown with a setting of 40-percent tail reduction resulted in a time-to-double amplitude of 1.33 sec in the destabilization portion of the quasi-tailless mode. The 50-percent tail reduction setting resulted in a time-to-double amplitude of 0.92 sec. This result compares to design goals of 1.28 sec and 0.83 sec obtained for a system without the lags in the angle-of-sideslip feedback path. Assessing the effect of the deadband in the sideslip feedback path is difficult because of its nonlinear nature. The sideslip excursions encountered during the power approach testing were within $\pm 1.5°$. The amount of turbulence experienced during the approach tasks was light. The pilot referred to these conditions as “clear air.”

A simulation study was initiated in an attempt to further determine the significance of the lags and deadband in the sideslip feedback path. The nonlinear simulation was changed so that true angle of sideslip was used for the destabilization paths. Meanwhile, the restabilization paths continued to use the corrupted sideslip measurement. Approaches were then flown on the piloted simulation with moderate turbulence and a quasi-tailless setting of

60-percent tail reduction. To ensure that control power issues did not mask the sensor-related issues, the drag of the X-31A simulation was arbitrarily increased. The approach task could then be flown with increased throttle settings to provide increased control power. Surprisingly, the deadband and lag in the sideslip feedback were barely perceptible to the pilot. When back-to-back comparisons of the baseline and modified simulations were made, these effects were noticeable; however, they did not significantly interfere with the precision approach task. The pilot noted a slight increase in the amount of stick input required. The baseline simulation appeared to be more responsive to smaller inputs.

The precision approach flight test data provided a good example of thrust vectoring with dynamic throttle inputs. The accuracy of the thrust estimation algorithm in the presence of rapid throttle movements is questionable. Although it used a direct measurement of pressure, the thrust estimator is based on a simplified model of the steady-state relationship between nozzle pressure ratio, nozzle exit area, and throttle position. The situation was further exacerbated by the presence of a filter on the thrust estimation output. The filter was installed to reduce noise and smooth failure transitions. If one assumes the unfiltered algorithm output is correct, the error between the unfiltered thrust estimation and filtered thrust estimation can be calculated. Figure 13 shows this error for a typical precision approach pass. The error was quite variable and up to 4 dB. With military specifications (ref. 13) for stability margin requirements of 6 dB, this error could be significant. The stability margin for the thrust vector loop in quasi-tailless mode was typically on the order of 20 dB for the X-31A airplane. As a result, variations on the order of 4 dB produced no noticeable reduction in stability.

Ground Attack Task

Several ground attack runs were flown by three pilots over five flights. Table 3 lists the pilot ratings. The airplane in basic mode was flown in back-to-back comparison with the quasi-tailless mode set at up to 60-percent tail size reduction. The change in roll performance was quite noticeable. One pilot commented that “the roll-in before the pull-down was executed at 320 to 330 KIAS at around 5° AOA. The roll performance was adequate for this phase of the tactical attack. The rollout for target acquisition was executed during the four runs at 290 to 300 KIAS at AOA varying between 16° and 5°. At AOA above 7°, the roll rate was considerably reduced compared to the basic mode. The roll performance was not adequate for this phase of the tactical attack.”

Table 3. Ground attack pilot ratings.

Flight number	Glide slope	Tail reduction setting, %	CHR gross acquisition	CHR fine tracking
287	45°	50 and 60	5	3
287	15° pop-up	0	5	2
		30, 40, 50, 60	5	3
288	45°	50	---	3
288	15° pop-up	Basic	---	2
		50 and 60	---	3
290	15° ATLAS	60	4	3
290	45°	Basic and 60	4	2
290	15° pop-up	Basic and 60	4	2
291	15° ATLAS	50	---	3
291	15° pop-up	50	---	---

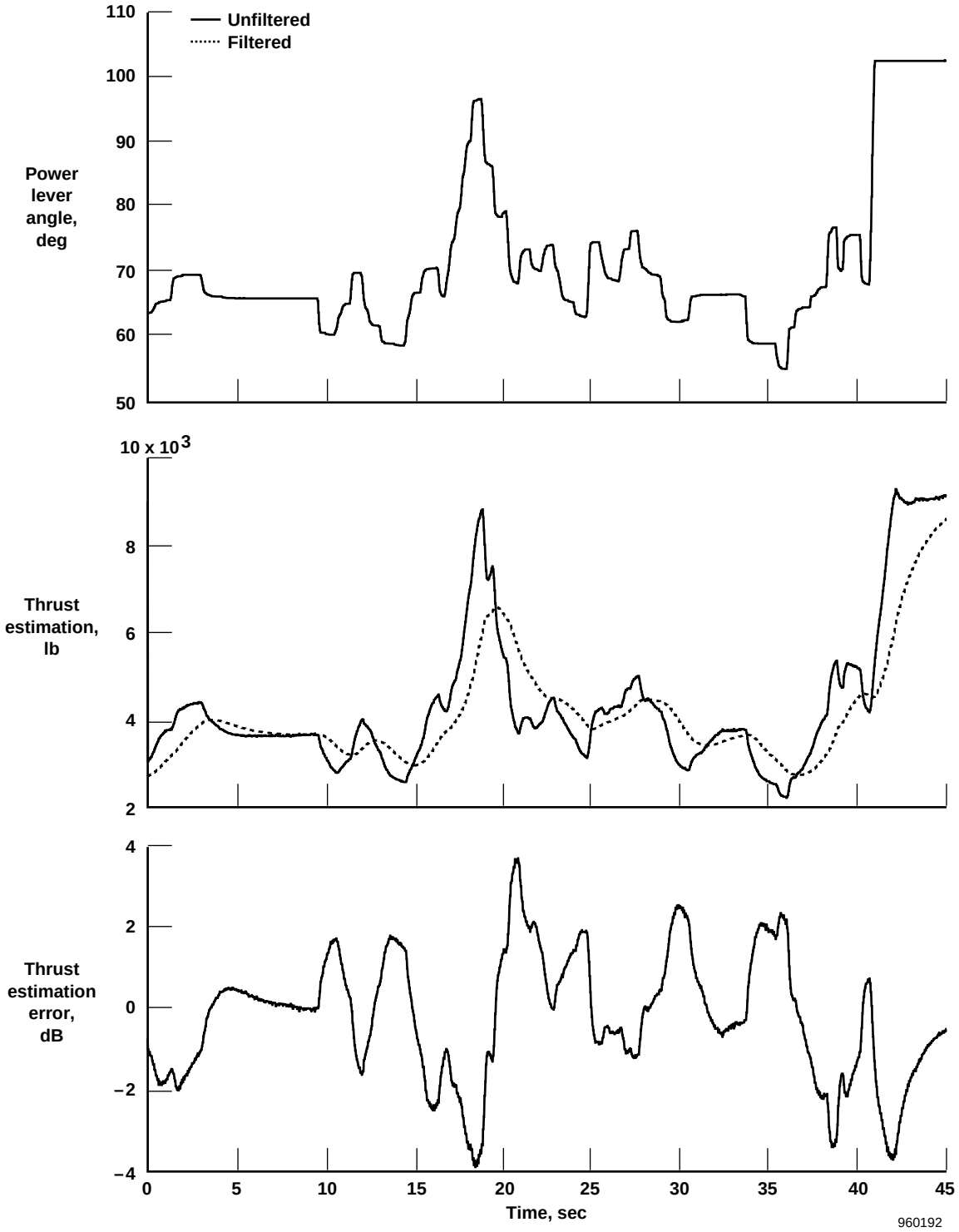

Figure 13. Errors introduced by filtering the thrust estimation calculation (representative X-31A precision approach run).

In addition, the pilot recommended, “to increase the roll performance during the phases when the aircraft is rolled at 7° AOA and more, a higher PLA should be used.” This modified approach to the ground attack was flown on subsequent flights. With the new technique, “roll at power settings of up through military rate thrust during the roll-in and gross acquisition phases of all attack profiles was markedly improved,” the pilot noted.

Based on the X-31A results, future tailless aircraft designs will require a higher level of interaction between engine power setting and the flight control system than exists in current designs. Relying on a pilot to limit his roll inputs for low-power settings is unreasonable. Restricting the roll commands to those controllable by the lowest power setting does not provide a feasible option. Automatic tailoring of the roll command with thrust available will be required to prevent inadvertent aircraft departures. This relationship between performance and thrust level imposes a requirement for a reliable, redundant thrust estimation algorithm. A system which automatically increases thrust when large yawing moments are required would be ideal for future applications. Such systems would also have to deploy drag devices to control longitudinal acceleration. Lead compensation might be required because the control power is required for roll initiation, and lags are associated with thrust spool-up times. Deploying the speedbrakes on the X-31A airplane allowed for improved control power; unfortunately, the speedbrakes also decreased the directional stability which increased the demand on the thrust vector system.

Figure 14 shows an aggressive roll-out for gross acquisition of a ground target and a 45° bomb run. The pilot commented, “during the rollout a β [angle of sideslip] buildup to $-2°$ was observed which did not disengage, QT [the quasi-tailless mode] but affected target acquisition with an overshoot.” The nonlinear simulation generally does a good job of reproducing the flight results; however, the sideslip excursion shown by the simulation was approximately one-half that observed in flight. This test was flown with the noseboom which did not exhibit any significant deadband.

The flight data time segment around the angle-of-sideslip buildup of figure 14 is expanded and shown in figure 15. The small sideslip buildup partially results from the fact that the thrust vector system is approaching its rate and position limits. With the relatively low-power setting and small nozzle area, slightly more than full travel and higher rates would have been required to correctly coordinate the roll input. Figure 15 shows paddle 3 momentarily rate limited and then position limited which allowed increased negative sideslip buildup. The position limit reached by paddle 3 was 34°. The control system limits the thrust vector deflection to maintain the paddles within their hardware command limits of 35°. In this case, the software limit was slightly more restrictive than the hardware limit.

An accurate simulation of the angle-of-sideslip excursion requires an improved model of the thrust vector system control power. Figure 16 shows that the thrust estimation from the flight data was 80 percent of that shown by the nonlinear simulation. Neither the nozzle area nor the turbine discharge pressure were accurately predicted for the ground attack profile. The shape of the turbine discharge pressure curve from simulation matched the flight data. These flight data, however, showed a bias in turbine discharge pressure which accounts for the majority of the error between simulation and flight-measured thrust estimation. The differences in nozzle area, in this case, were not large enough to significantly affect the thrust estimation calculation or the plume boundary calculation. The reason for the change in the nozzle area shown in figure 16 is not fully understood. This change was not predicted by the nonlinear simulation engine model or a more detailed stand-alone engine model, yet this change was consistently observed during the relatively rapid altitude change in the 45° dive. The ability of the thrust estimator to work in the presence of this anomaly is unknown.

The nonlinear simulation gross thrust and thrust estimation were set equal to the in-flight thrust estimation value in an effort to improve agreement in angle of sideslip. The sideslip excursion was still not reproduced. The ratio between gross thrust and estimated thrust is an important quantity for accurate simulation. The difference between actual and estimated thrust determines whether the system over or under compensates with the thrust vector system.

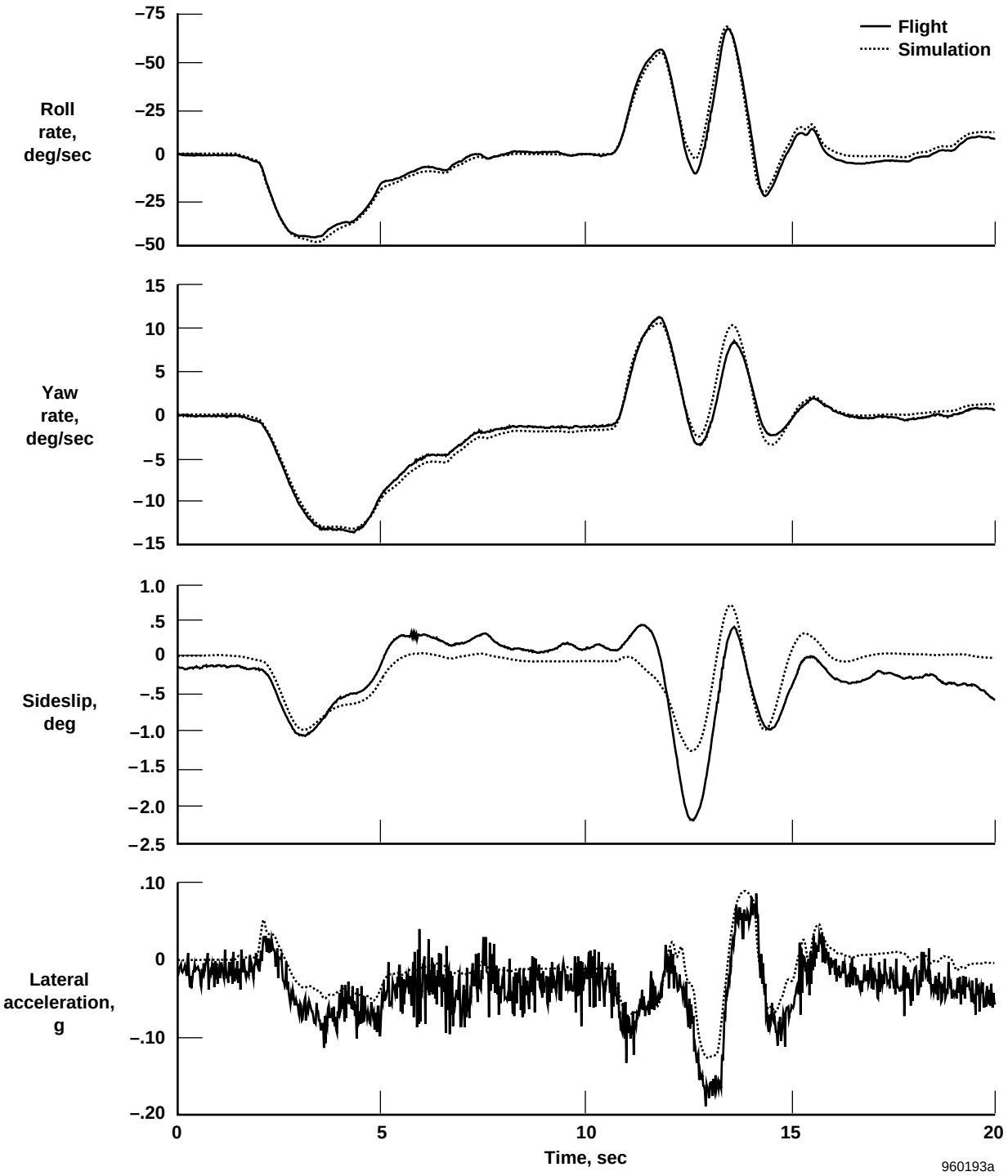

Figure 14. Ground attack rollout with 50-percent tail reduction setting (comparison of flight data to a nonlinear simulation).

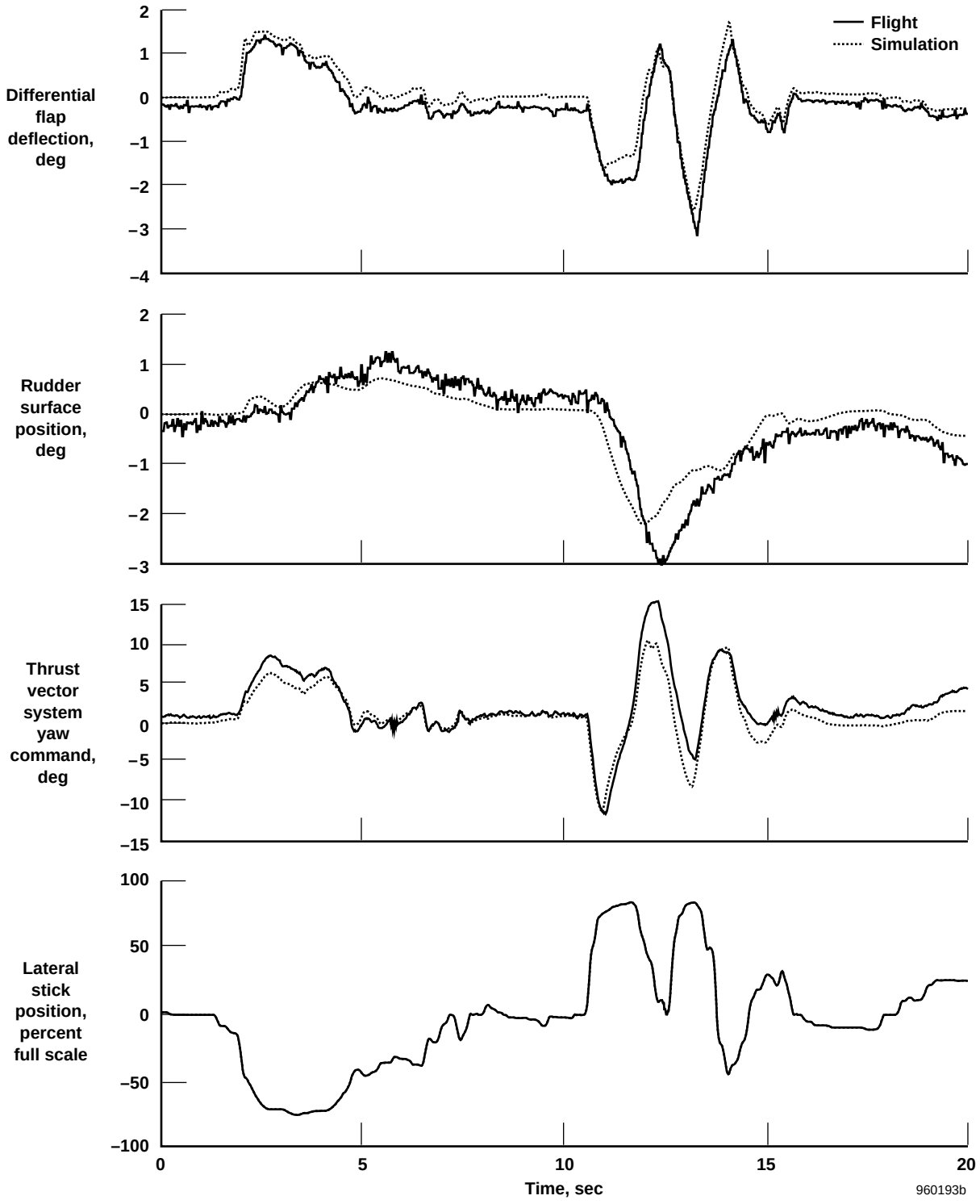

Figure 14. Concluded.

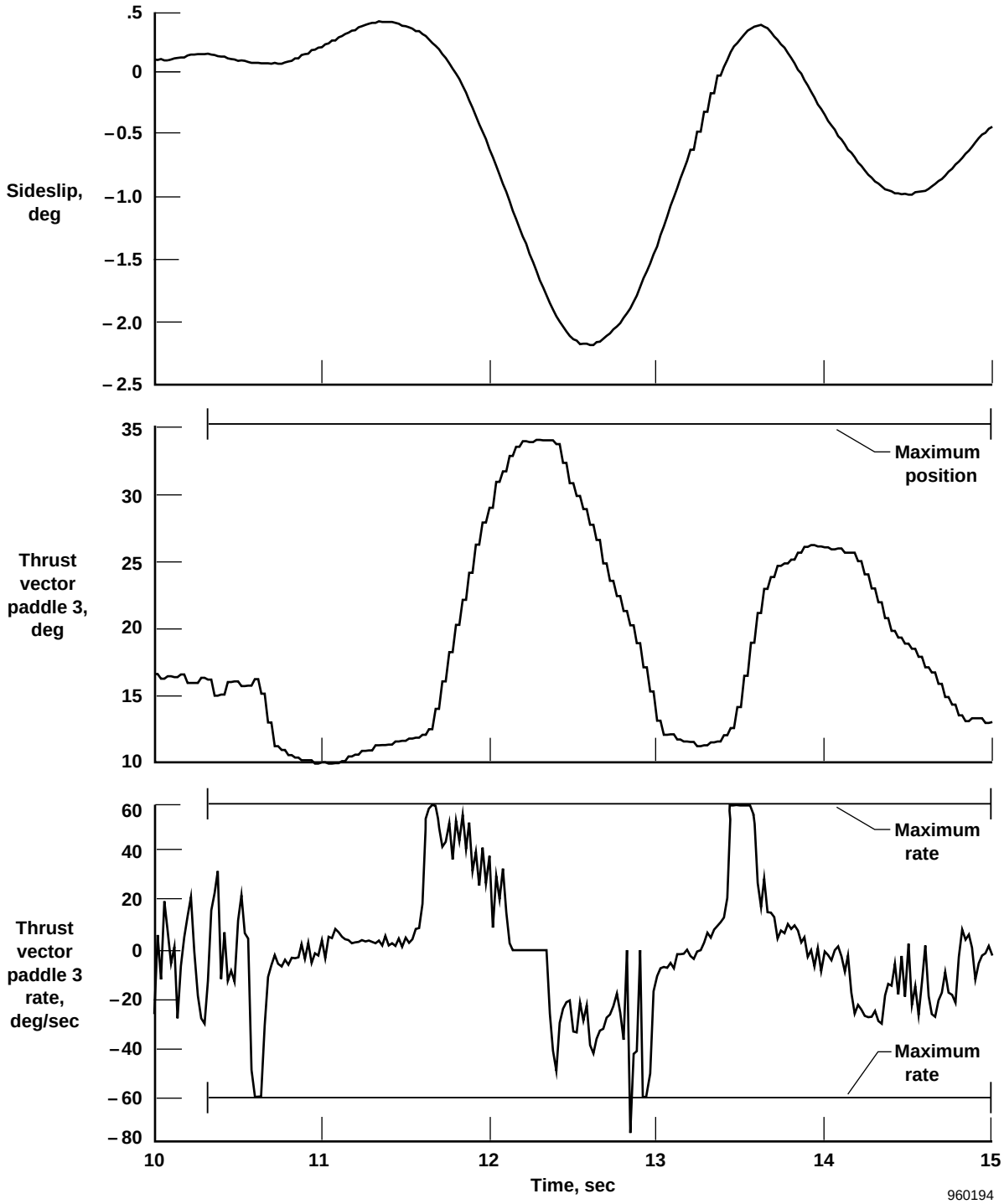

Figure 15. Ground attack rollout with 50-percent tail reduction setting (expanded view of sideslip excursion).

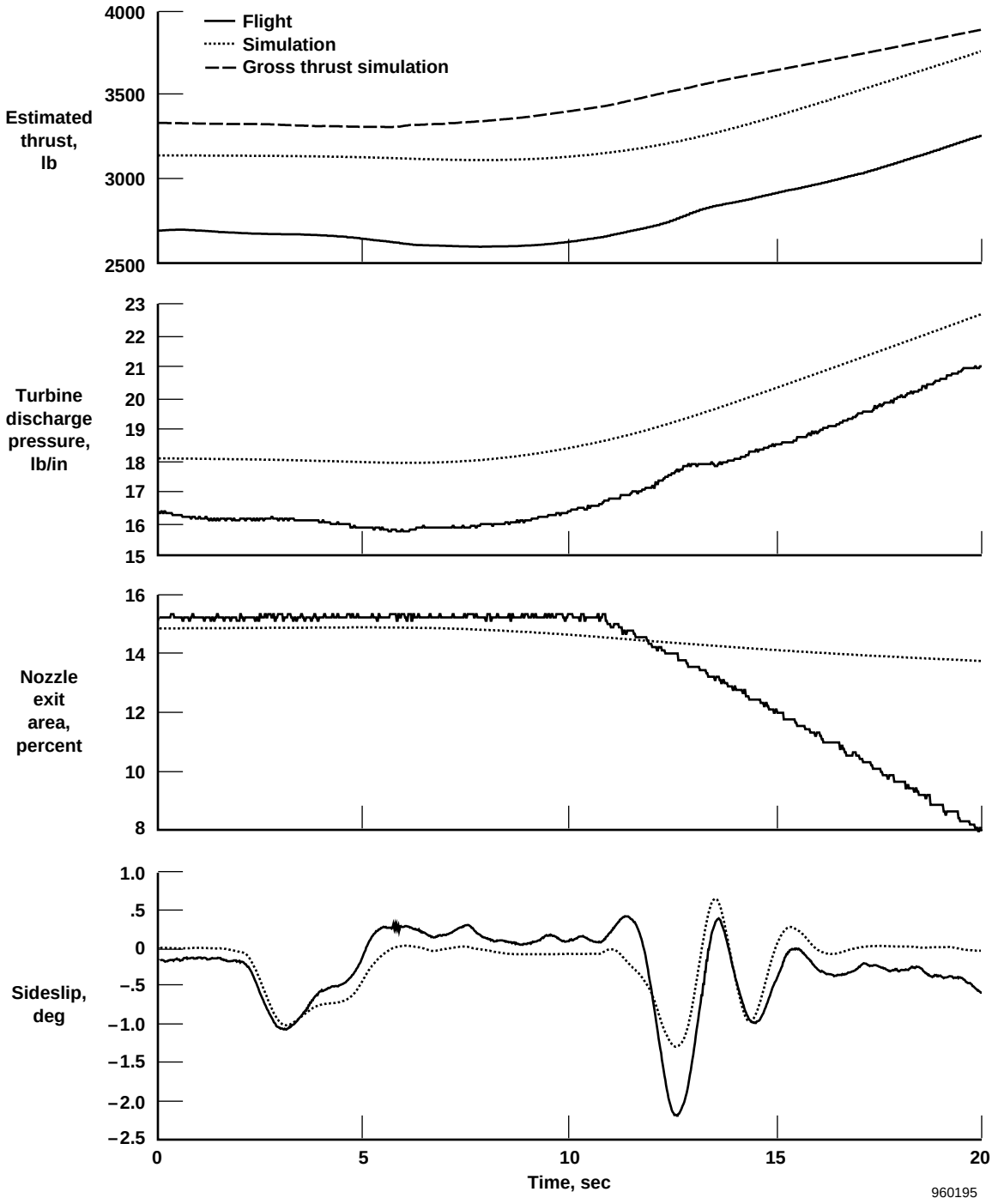

Figure 16. Ground attack rollout with 50-percent tail reduction setting (thrust estimation algorithm).

To reproduce the sideslip excursion observed in figure 14 required a further reduction of 20 percent on the gross thrust value in the simulation (fig. 17). The reduced thrust causes a mismatch between the rudder and thrust vector control power which results in the sideslip excursion. A similar mismatch in control power could be obtained by increasing the rudder effectiveness. With a 40-percent increase in rudder control power, a similar sideslip excursion was reproduced (fig. 18).

Neither of these simulations fully reproduced the behavior observed in flight. While the sideslip match was improved during the roll-out, the match was somewhat degraded for other parameters at other times. Some combination of these changes is probably the real cause.

Variations in gross thrust throughout the life cycles of engines are not uncommon. In addition, force transducer measurements on the X-31A thrust vector paddles indicated a possible loss in plume-turning effectiveness for plume-turning angles greater than 12°. The flight control system should be able to account for these types of variations for future applications.

The ground attack flight tests illustrated the increased interdependence of the flight control system, aerodynamics, and propulsion for a thrust-vector-controlled airplane compared to conventional airplanes. The F-18 High-Angle-of-Attack Research Vehicle (HARV) program also found significant levels of thrust-vector-induced aerodynamic changes (ref. 14). The flow entrainment on the vertical tails at high-power settings and large vectoring angles changed the vertical tail aerodynamic effectiveness. The HARV was manufactured by McDonnell Douglas Corporation, St. Louis, Missouri.

LESSONS LEARNED

The following is a summary of the lessons learned from the X-31A quasi-tailless flight test experiment.

- Thrust vectoring is a viable control effector which can replace the functions of a vertical tail and rudder control surface.
- Pilot comments indicate that no difference in handling qualities exists as long as the task and destabilization level did not demand more control power than was available.
- The amount of roll acceleration required is an important quantity in determining the level of directional instability that can be controlled.
- An increased level of interaction between the engine and flight control system will be required for future reduced tail or tailless vehicles with thrust vector control.
- Minor sensor feedback characteristics, such as delays and deadbands, can have a larger than expected affect when angle of sideslip is used as a destabilizing feedback.
- The thrust estimation algorithm is an important component of a successful integration of thrust vectoring into the control system.
- Using drag devices to fly at an increased power setting can introduce additional directional instability.
- Large thrust vector control deflections may significantly influence the aerodynamic flow over the airplane.
- Early integration of thrust vectoring into the design process maximizes the achievable benefits.

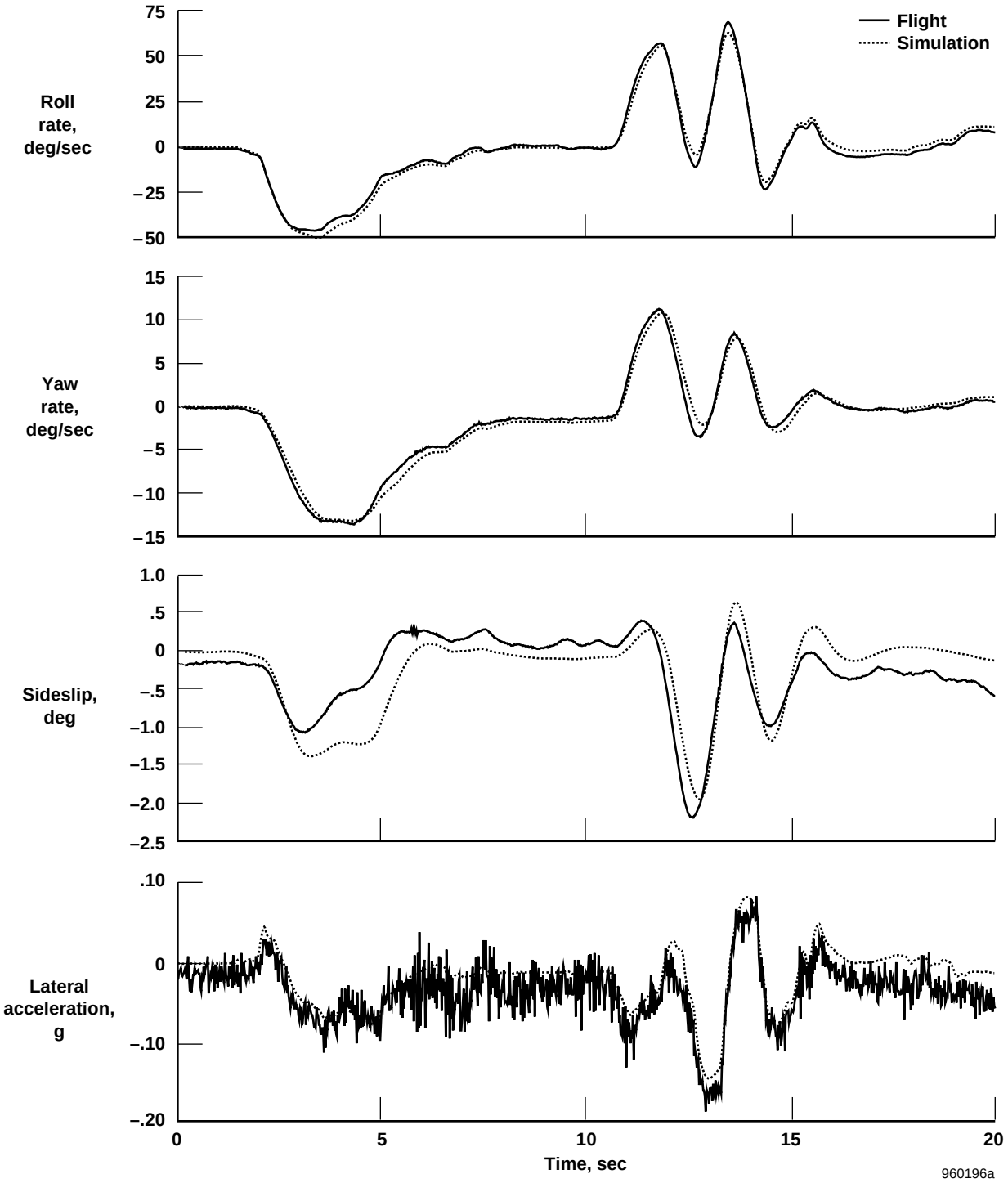

Figure 17. Ground attack rollout with 50-percent tail reduction setting (comparison of flight data to nonlinear simulation with reduced gross thrust.)

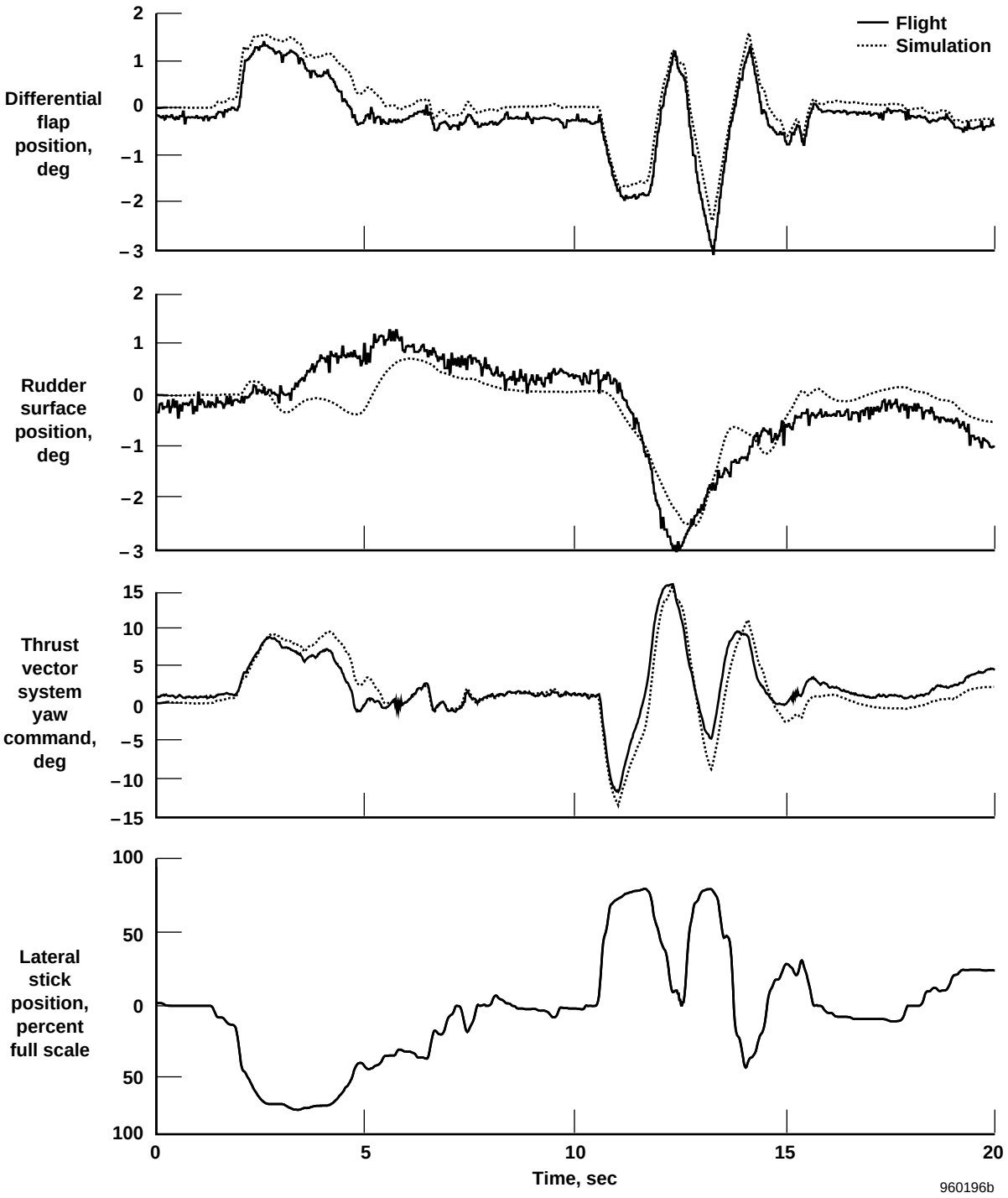

Figure 17. Concluded.

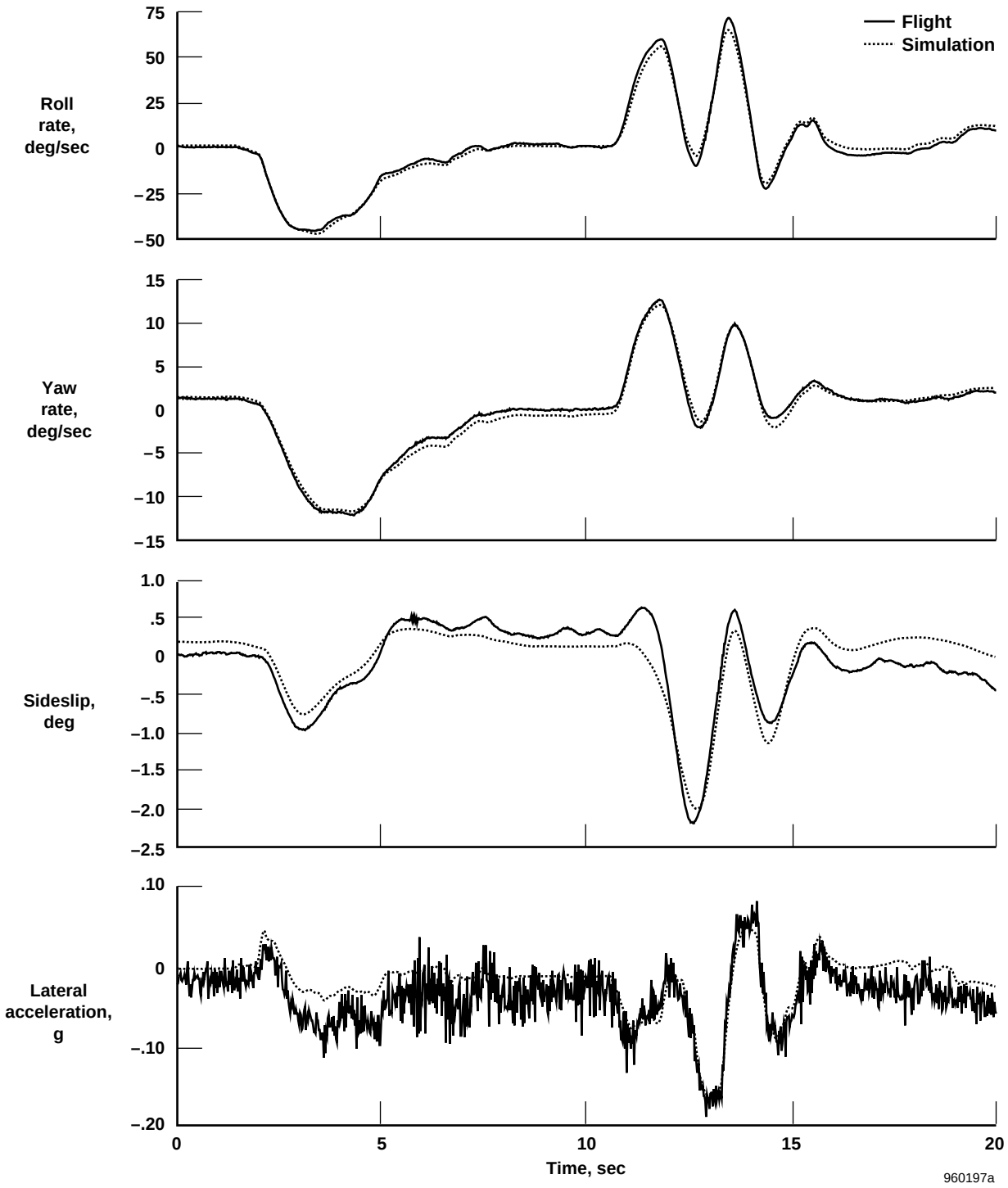

Figure 18. Ground attack rollout with 50-percent tail reduction setting (comparison of flight data to a nonlinear simulation with increased rudder control power).

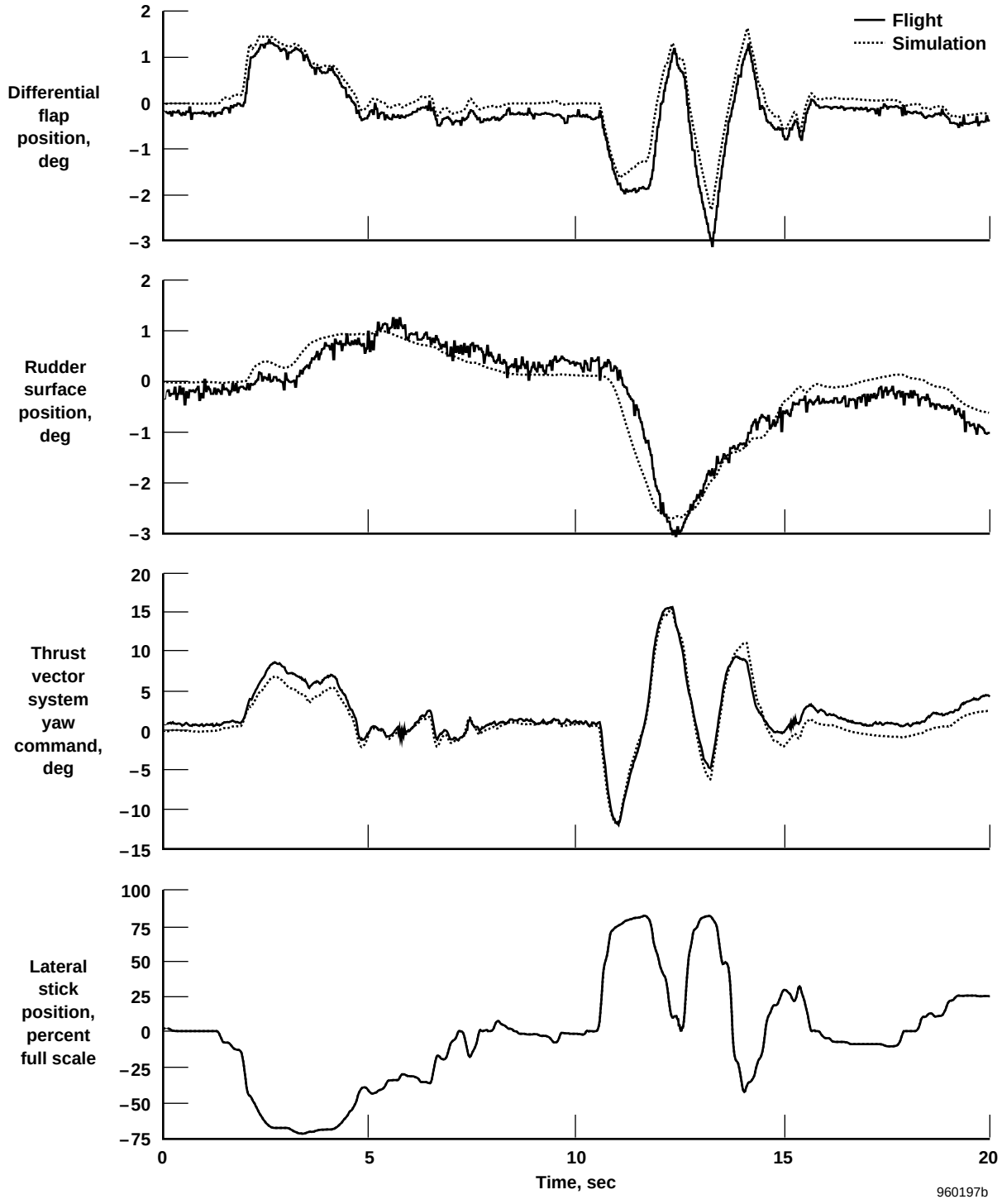

Figure 18. Concluded.

CONCLUDING REMARKS

The X-31A quasi-tailless flight test experiment successfully demonstrated the ability to use thrust vectoring to replace the functions of stabilization and turn coordination usually required of a rudder and vertical tail. Pilot comments indicated no difference in handling qualities as long as the task and destabilization level did not demand more control power than was available. At low thrust settings and high roll accelerations, the thrust vector system reached rate and position saturation. An increased level of interaction between the engine and flight control system will be required for future reduced tail or tailless vehicles with thrust vector control. This experiment helped to introduce thrust vectoring as a new design dimension for future aircraft.

The supersonic quasi-tailless test showed that maneuvering typically required of transport aircraft, such as future versions of supersonic civilian transports, could be controlled by thrust vectoring for fairly high levels of instability. A tail reduction setting of 70 percent was flown. This setting was equivalent to an approximately 170-msec, time-to-double amplitude. The destabilize-only mode showed that the vehicle achieved levels of instability which were slightly less than the design goals. This result was primarily caused by an equivalent time delay of approximately 67 msec in the sideslip feedback path. In retrospect, this delay should have been accounted for in the models used to calculate the destabilization gains. In addition, these data showed what amounted to a deadband on the sideslip feedback path. This finding further confused the evaluation of the exact level of destabilization achieved in flight.

The precision approach testing provided a first look at using thrust vectoring at low-power settings. The flying qualities were consistent up to a tail reduction setting of 50 percent (approximately 0.92-sec, time-to-double amplitude). High throttle activity coupled with a lag on the thrust estimation algorithm resulted in errors in the thrust control loop gain as high as 4 dB. These errors did not produce noticeable stability problems for the X-31A airplane because of the high loop gain margin. However, the study showed that an accurate redundant onboard thrust estimation algorithm is a requirement for an integrated engine and flight control system. Improved estimation of thrust changes resulting from rapid throttle movement is required, or a high stability margin requirement for the thrust vector loop should be imposed.

All precision approaches flown were in low atmospheric turbulence or clear air conditions. A limited nonlinear simulation study showed that even with the deadband and lag in the sideslip feedback path no significant handling qualities problems were introduced with simulated turbulence. However, the fidelity of the turbulence models was not extensively tested, and prediction of airplane response to turbulence is usually difficult. Issues of ride qualities and disturbance rejection in the presence of atmospheric turbulence would be better addressed with a real tailless or reduced tail vehicle.

Several ground attack profiles were flown. This task demanded large amplitude rolls in conjunction with low thrust settings. Tailoring the roll commands as a function of available yaw control power was required to avoid departing from coordinated flight. This tailoring introduces an increased level of interaction between the engine and flight control system. Even with reductions of as much as 50 percent (to approximately 120 deg/sec) on the maximum roll rate command and 65 percent (to approximately 210 deg/sec^2) on the roll acceleration command limit, some position and rate saturation were observed at a setting of 50-percent tail size reduction (approximately 0.92-sec, time-to-double amplitude).

Accurate prediction of when these saturations will occur requires higher fidelity engine models in the nonlinear simulation than the models that are typically used. Additional care should be taken to accurately model the inputs to the thrust estimation algorithm and the plume boundary location for a system with thrust vector paddles. The thrust estimation algorithm should be valid for degraded engine performance because large variations in performance can be expected over the life cycle of an engine.

During one ground attack run, a sideslip excursion was noted which resulted from a mismatch between thrust vector and rudder surface control power. The cause for the mismatch is unknown; however, simulating reduced thrust vector effectiveness or increased rudder effectiveness produces similar excursions in sideslip. Other thrust vectoring airplanes, such as the F-18 High Angle of Attack Research Vehicle, showed potential for interactions between the vehicle aerodynamics and the thrust vectoring system. This interaction results from flow entrainment on the vertical tail caused by large vectoring angles.

Future tailless vehicles will have the advantage of production thrust vectoring systems based on axisymmetric nozzles. In addition, a tailless vehicle configured to minimize directional instability tends to be neutrally stable rather than directionally unstable. This configuration would reduce the demands placed on a thrust vector system. A production thrust vectoring system would reduce concerns over such issues as where the plume boundary is, how much thrust is lost from vectoring, and what is the achieved plume deflection angle which were of more concern with a thrust vector paddle system. However, a good thrust estimator and an increased level of engine and control system interaction will be required.

In addition to these issues, a reasonable approach to the engine-out failure condition must be developed. If this approach includes emergency deployed devices to regain directional stability, the cost and weight must be considered. The cost and weight of adding a thrust vector system are being reduced by improved designs of production axisymmetric thrust vectoring engines.

The X-31A quasi-tailless flight test experiment showed that tailless and reduced tail fighter aircraft are definitely feasible. When the capability is designed in from the beginning, the benefits of reduced drag, structural complexity, and radar cross-section have the potential to outweigh the added complexity required.

Dryden Flight Research Center
National Aeronautics and Space Administration
Edwards, California, March 14, 1996.

REFERENCES

1. Herbst, W.B., "X-31A at First Flight," *Flying Qualities*, AGARD CP-508, Feb. 1991, p.p. 29-1–29-8.

2. Huber, P., Weiss, S., and Galleithner, H., "X-31A Initial Flying Qualities Results Using Equivalent Modeling Flight Test Evaluation Techniques," AIAA-91-2891, Aug. 1991.

3. Huber, Peter and Seamount, Patricia, "X-31 High Angle of Attack Control System Performance," *NASA Dryden Flight Research Center, Fourth High Alpha Conference*, vol. 2, NASA CP-10143, July 12–14, 1994.

4. Cantor, David E. and Groves, Allen W., "X-31 Tactical Utility—Initial Results," *Technologies for Highly Maneuverable Aircraft*, Flight Mechanics Panel Symposium AGARD, Annapolis, Maryland, Oct. 18–23, 1993.

5. Eubanks, D., Gütter, R., and Lee, B., "X-31 CIC Flight Test Results," *Four Power Senior Nation Representative Full Envelope Agility Workshop*, Elgin AFB, Florida, Mar. 1995.

6. Beh, H. and Hofinger, G., "X-31A Control Law Design," *Technologies for Highly Maneuverable Aircraft*, AGARD CP-548, Mar. 1994, p.p. 13-1–13-9.

7. Norlin, Ken A., *Flight Simulation Software at NASA Dryden Flight Research Center*, NASA TM-104315, 1995.

8. Huber, Peter and Schellenger, Harvey G., "X-31 Quasi-Tailless Flight Demonstration," *Fourth High Alpha Conference, NASA Dryden Flight Research Center*, vol. 2, NASA CP-10143, July 12–14, 1994.

9. Loria, Christopher J., Kelly, Mark K., and Harney, Ron, "X-31A Quasi-Tailless Evaluation," *27th European Symposium of the Society of Flight Test Engineers (SETP)*, May 3–6, 1995.

10. Huber, Peter, "Control Law Design for Tailless Configurations and In-Flight Simulation Using the X-31 Aircraft," AIAA-95-3199, Aug. 1995.

11. Shafer, M.F., Koehler, R., Wilson, E.M., and Levy, D.R., *Initial Flight Test of a Ground Deployed System for Flying Qualities Assessment*, NASA TM-101700, 1989.

12. Cooper, George E. and Harper, Robert P., *The Use of Pilot Rating in the Evaluation of Aircraft Handling Qualities*, NASA TN D-5153, 1969.

13. Military Specification: "Flying Qualities of Piloted Airplanes," MIL-F-8785C, Nov. 1980.

14. Bowers, Albion H., Noffz, Gregory K., Grafton, Sue B., Mason, Mary L., and Peron, Lee R., *Multiaxis Thrust Vectoring Using Axisymmetric Nozzles and Postexit Vanes on an F/A-18 Configuration Vehicle*, NASA TM-101741, 1991.

REPORT DOCUMENTATION PAGE

Form Approved
OMB No. 0704-0188

1. AGENCY USE ONLY (Leave blank)	2. REPORT DATE	3. REPORT TYPE AND DATES COVERED
	June 1996	Technical Paper

4. TITLE AND SUBTITLE

The X-31A Quasi-Tailless Flight Test Results

5. FUNDING NUMBERS

WU 505-68-30

6. AUTHOR(S)

John T. Bosworth and P. C. Stoliker

7. PERFORMING ORGANIZATION NAME(S) AND ADDRESS(ES)

NASA Dryden Flight Research Center
P.O. Box 273
Edwards, California 93523-0273

8. PERFORMING ORGANIZATION REPORT NUMBER

H-2091

9. SPONSORING/MONOTORING AGENCY NAME(S) AND ADDRESS(ES)

National Aeronautics and Space Administration
Washington, DC 20546-0001

10. SPONSORING/MONITORING AGENCY REPORT NUMBER

NASA TP-3624

11. SUPPLEMENTARY NOTES

Presented at the Second Test and Evaluation International Aerospace Forum, London, England, June 25–27, 1996.

12a. DISTRIBUTION/AVAILABILITY STATEMENT

Unclassified—Unlimited
Subject Category 08

12b. DISTRIBUTION CODE

13. ABSTRACT (Maximum 200 words)

A quasi-tailless flight investigation was launched using the X-31A enhanced fighter maneuverability airplane. In-flight simulations were used to assess the effect of partial to total vertical tail removal. The rudder control surface was used to cancel the stabilizing effects of the vertical tail, and yaw thrust vector commands were used to restabilize and control the airplane. The quasi-tailless mode was flown supersonically with gentle maneuvering and subsonically in precision approaches and ground attack profiles. Pilot ratings and a full set of flight test measurements were recorded. This report describes the results obtained and emphasizes the lessons learned from the X-31A flight test experiment. Sensor-related issues and their importance to a quasi-tailless simulation and to ultimately controlling a directionally unstable vehicle are assessed. The X-31A quasi-tailless flight test experiment showed that tailless and reduced tail fighter aircraft are definitely feasible. When the capability is designed into the airplane from the beginning, the benefits have the potential to outweigh the added complexity required.

14. SUBJECT TERMS

Aircraft stability; Flight test; Flight research; Flight simulation; Quasi-tailless airplanes; Rudder control; Tailless aircraft; Thrust vector; X-31 Airplane; Yaw control

15. NUMBER OF PAGES

43

16. PRICE CODE

A03

17. SECURITY CLASSIFICATION OF REPORT	18. SECURITY CLASSIFICATION OF THIS PAGE	19. SECURITY CLASSIFICATION OF ABSTRACT	20. LIMITATION OF ABSTRACT
Unclassified	Unclassified	Unclassified	Unlimited